

Copyright Warning & Restrictions

The copyright law of the United States (Title 17, United States Code) governs the making of photocopies or other reproductions of copyrighted material.

Under certain conditions specified in the law, libraries and archives are authorized to furnish a photocopy or other reproduction. One of these specified conditions is that the photocopy or reproduction is not to be “used for any purpose other than private study, scholarship, or research.” If a user makes a request for, or later uses, a photocopy or reproduction for purposes in excess of “fair use” that user may be liable for copyright infringement,

This institution reserves the right to refuse to accept a copying order if, in its judgment, fulfillment of the order would involve violation of copyright law.

Please Note: The author retains the copyright while the New Jersey Institute of Technology reserves the right to distribute this thesis or dissertation

Printing note: If you do not wish to print this page, then select “Pages from: first page # to: last page #” on the print dialog screen

The Van Houten library has removed some of the personal information and all signatures from the approval page and biographical sketches of theses and dissertations in order to protect the identity of NJIT graduates and faculty.

ABSTRACT

PREPARATION AND CHARACTERIZATION OF REACTIVE COMPOSITES COMBINING BORON WITH MIXED OXIDES

by

Purvam Mehulkumar Gandhi

Thirteen liquids have been explored as Process Control Agents (PCAs) for high-energy mechanical milling of two metal oxide powders, CuO and Bi₂O₃, with the practical purpose to reduce the sizes of powder particles and refine their crystal structure. Multiple liquid properties have been considered to analyze their effect on evolution of both particle and crystallite sizes during milling for each oxide. Experimental data were analyzed using the δ -AICc (Akaike Information criterion) correlation function applied to linear relations between liquid properties and powder characteristics. Multiple linear correlation models were ranked based on the highest log-likelihood and the lowest δ -AICc values. Liquid properties affecting milling outcomes in each case were identified; the data also identified specific liquids that are most effective PCAs. Respectively, a PCA was selected to prepare and characterize B-based thermites with both oxides forming binary oxidizers with varied compositions. Thermal analysis of these reactive composites was conducted along with the ignition and combustion experiments. It was observed that thermites with binary oxidizers had distinct characteristics of low-temperature oxidation; however, the differences between different thermites diminished during their combustion tests.

**PREPARATION AND CHARACTERIZATION OF REACTIVE COMPOSITES
COMBINING BORON WITH MIXED OXIDES**

by
Purvam Mehulkumar Gandhi

**A Thesis
Submitted to the Faculty of
New Jersey Institute of Technology
in Partial Fulfillment of the Requirements for the Degree of
Master of Science in Chemical Engineering**

**Otto H. York Department of
Chemical and Materials Engineering**

December 2020

Blank Page

APPROVAL PAGE

**PREPARATION AND CHARACTERIZATION OF REACTIVE COMPOSITES
COMBINING BORON WITH MIXED OXIDES**

Purvam Mehulkumar Gandhi

Dr. Edward L. Dreizin, Thesis Advisor Date
Distinguished Professor of Chemical Engineering, NJIT

Dr. Mirko Schoenitz, Committee Member Date
Research Professor of Chemical Engineering, NJIT

Dr. Murat Guvendiren, Committee Member Date
Assistant Professor of Chemical Engineering, NJIT

BIOGRAPHICAL SKETCH

Author: Purvam Mehulkumar Gandhi

Degree: Master of Science

Date: December 2020

Undergraduate and Graduate Education

- Master of Science in Chemical Engineering,
New Jersey Institute of Technology, Newark, NJ, 2020
- Bachelor of Technology in Chemical Engineering,
Nirma University, Ahmedabad, Gujarat, India, 2019

Major: Chemical Engineering

This thesis is dedicated to my special ones;
parents, grandparents, and friends.

ACKNOWLEDGEMENT

I would like to take this opportunity to thank all the people who have helped me to be who I am today. I am grateful for all of them to have helped me and I would always remember them. Here is the list of the key members without whose help, this project would not be possible.

First of all, with great admiration, respect, and gratitude I would like to acknowledge Dr. Edward Dreizin, my advisor, without his help and guidance, this project was not possible. He had helped me and guided me throughout my graduate study. His monumental contribution to this research field has always inspired me. I would like to thank him for taking a keen interest and detailed approach to my work.

I would like to thank and appreciate my committee members, Dr. Murat Guvendiren, and Dr. Mirko Schoenitz for all the suggestions and help they have provided during this project. I thank Dr. Murat Guvendiren for always being helpful and suggesting new ideas in this project. Dr. Mirko Schoenitz has always helped me with his technical abilities to help me give thorough knowledge about all the characterization techniques.

I would like to thank all my fellow lab-mates for their guidance especially Siva Kumar Valluri. He has been a great support for me throughout my thesis project. He has helped me to get through all the difficulties and provided sheer willingness to help me out during my lows. I am extremely grateful for all the efforts he had made to make me understand the basic technical concepts during my time at the lab. I have the uttermost respect for his discipline and commitment in his work.

Last but not the least, this project would not be completed without the help, support, love, and prayers from my parents, family members, teachers, and friends. I shall always be grateful for all the care and concerns they have shown on me.

TABLE OF CONTENTS

Chapter	Page
1 INTRODUCTION.....	1
2 EFFECT OF SOLVENT USED AS PROCESS CONTROL AGENT ON PROPERTIES OF BALL MILLED POWDERS	4
2.1 Experimental.....	4
2.1.1 Material and Material Preparation	4
2.1.2 Material Characterization	6
2.2 Results.....	6
2.2.1 Compositional Analysis and Crystallite Properties.....	6
2.2.2 Particle Size Distribution (PSD) Analysis.....	8
2.3 Discussion	12
2.3.1 Correlation between solvent properties and milled powder properties.....	12
3 EFFECT OF $\text{Bi}_2\text{O}_3\cdot\text{CuO}$ BINARY OXIDIZER ON BORON'S IGNITION AND COMBUSTION IN FUEL-RICH COMPOSITION	24
3.1 Experimental.....	24
3.1.1 Experimental Approach.....	24
3.1.2 Preparation of Oxidizers.....	25
3.1.3 Preparation of Boron-Oxidizer Reactive Powders.....	28
3.1.4 Material Characterization	29
3.1.5 Heated Filament Experiment	30

TABLE OF CONTENTS

(continued)

Chapter	Page
3.1.6 Particle Combustion Experiments.....	31
3.1.7 Aerosolized Particles Collection and Sizing.....	32
3.2 Results and Discussion.....	33
3.2.1 Oxidizer Characterization.....	33
3.2.2 Boron-Oxidizer Powder Morphology	41
3.2.3 Thermal Analysis	45
3.2.4 Ignition Temperature.....	53
3.2.5 Correlation of ignition temperature with reactions observed in thermos-analytical experiments	54
3.2.6 Particle Combustion in Air	58
4 SUMMARY AND FUTURE WORK	63
5 REFERENCES	67

LIST OF TABLES

Table	Page
2.1 Chemical Formula, Molecular Structure of the Solvents used in this Study	5
2.2 The Crystallite Size and Surface Area based Bulk Powder Property (D_{50}) of Milled Bi_2O_3 and CuO Powders Obtained by Milling in Various Solvents Employed as Process Control Agents under Identical Conditions	13
2.3 Properties of the PCAs Used in this Study.....	14
2.4 Coefficients of Linear Models Describing Measured Results as Function of PCA Properties for Bi_2O_3	17
2.5 Coefficients of Linear Models Describing Measured Results as Function of PCA Properties for CuO	19
3.1 Targeted Oxidizer Compositions and their Nomenclature	24
3.2 Targeted Synthesized Oxidizer Compositions and the Required Mass of their Corresponding Nitrates to obtain 12g of Oxidizer	26
3.3 Targeted Composition of Boron·Oxidizer Samples	29
3.4 Prepared Compositions per Vial of Boron·Synthesized-Oxidizer Samples	38
3.5 Theoretical and Experimentally Observed Mass Gains and Degree of Oxidation Achieved by B·Synthesized Oxidizers	46
3.6 Theoretical and Experimentally Observed Mass Gains and Degree of Oxidation Achieved by B·Milled Oxidizers	48

LIST OF FIGURES

Figure	Page
2.1 XRD traces of freshly milled powders of bismuth (III) oxide milled in different solvents under identical conditions. The solvents used as PCA are listed beside their respective trace	7
2.2 XRD traces of freshly milled powders of copper (II) oxide milled in different solvents under identical conditions. The solvents used as PCA are listed beside their respective traces	8
2.3 The particle size distribution of bismuth (III) oxide powders milled in different solvents under identical conditions	10
2.4 The particle size distribution of copper (II) oxide powders milled in different solvents under identical conditions	11
2.5 Correlation between log-likelihood and δ -AICc values for Bi_2O_3 powder based on (a) surface based median particle size and (b) crystallite size	18
2.6 Correlation between log-likelihood and δ -AICc values for CuO powder based on (a) surface based median particle size and (b) crystallite size	20
2.7 Observed and predicted milling outcomes of (A) surface based particle size and (B) crystallite size for Bi_2O_3	22
2.8 Observed and predicted milling outcomes of (A) surface based particle size and (B) crystallite size for CuO	23
3.1 Particle size distribution of (A) freshly milled oxidizers (B) freshly synthesized oxidizers and (C) milled synthesized oxidizers	34
3.2 Compositional analysis of $\text{Bi}_2\text{O}_3 \cdot \text{CuO}$ milled oxidizers.....	35
3.3 Background subtracted XRD traces of freshly prepared milled oxidizers.....	35
3.4 Compositional analysis of $\text{Bi}_2\text{O}_3 \cdot \text{CuO}$ synthesized oxidizers.....	37
3.5 Background subtracted XRD traces of freshly prepared synthesized oxidizers	37
3.6 Compositional analysis of size reduced $\text{Bi}_2\text{O}_3 \cdot \text{CuO}$ synthesized oxidizers	39
3.7 Background subtracted XRD traces of milled synthesized oxidizers.....	39
3.8 Estimated Bi_2O_3 mass percentage in the prepared $\text{Bi}_2\text{O}_3 \cdot \text{CuO}$ binary oxidizers	40

LIST OF FIGURES
(continued)

Figure	Page
3.9 The SEM images of B-synthesized-oxidizers representative particles: (A) B·100CuO, (B) B·25Bi ₂ O ₃ ·75CuO, (C) B·50Bi ₂ O ₃ ·50CuO, (D) B·75Bi ₂ O ₃ ·25CuO and (E) B·100Bi ₂ O ₃ along with (F) magnified surface morphology of B·50Bi ₂ O ₃ ·50CuO particle	42
3.10 The SEM images of B-milled-oxidizers representative particles: (A) B·100CuO, (B) B·25Bi ₂ O ₃ ·75CuO, (C) B·50Bi ₂ O ₃ ·50CuO, (D) B·75Bi ₂ O ₃ ·25CuO and (E) B·100Bi ₂ O ₃ along with (F) surface morphology of large B·75Bi ₂ O ₃ ·25CuO particle.....	43
3.11 Particle size distribution of freshly prepared (A) B-synthesized-oxidizer and (B) B-milled-oxidizer samples	44
3.12 TG and corresponding DTA plots of B-synthesized oxidizer reactive composites heated at 5K/min in oxidative environment.....	46
3.13 TG and corresponding DSC plots of B-milled oxidizer reactive composites heated at 5 K/min in oxidative environment.....	47
3.14 The DTG plots of B-synthesized oxidizer and B-milled oxidizer reactive composites heated at 5K/min in oxidative environment.....	49
3.15 TG and corresponding DTA plots of B-synthesized oxidizer reactive composites heated at 40 K/min in inert environment	50
3.16 TG and corresponding DTA plots of B-milled oxidizer reactive composites heated at 40K/min in inert environment.....	51
3.17 The measurements obtained from thermal analysis runs: (A) Total mass gain in oxidative runs, (B) DTG peak intensity in oxidative runs, (C) Area under DSC/DTA peaks in oxidative runs, and (D) Area under DTA peak in inert runs, plotted as a function of Bi ₂ O ₃ in oxidizer	52
3.18 Ignition temperature of B-synthesized oxidizer samples in air as a function of heating rate	53
3.19 Ignition temperature of B-milled oxidizer samples in air as a function of heating rate	54
3.20 Kissinger plots correlating inverse ignition temperatures, 1/T, with the inverse temperatures of the onset of mass gain observed in the oxidizing TG runs. The vertical scale is a variable determined by the heating rate, HR.....	55

LIST OF FIGURES
(continued)

Figure	Page
3.21 The difference between the experimentally obtained inverse temperature for onset of mass gain and inverse temperature projected by extrapolating the kinetic trend for ignition for B-synthesized oxidizer composites to low heating rates	56
3.22 Kissinger plots correlating inverse ignition temperatures, $1/T$, with the inverse temperatures of the onset of mass gain observed in the oxidizing TG runs for B-milled oxidizer composites. The vertical scale is a variable determined by the heating rate, HR	57
3.23 The difference between the experimentally obtained inverse temperature for onset of mass gain and inverse temperature projected by extrapolating the kinetic trend for ignition for B-milled oxidizer composites to low heating rates	58
3.24 The representative emission pulses observed in laser-assisted particle combustion experiments in air for the prepared B-milled oxidizer samples	59
3.25 The burn time distributions of the prepared B-milled oxidizer samples obtained from particle combustion experiments in air	60
3.26 The aerosolized particle size distributions of the prepared B-milled oxidizer samples in the laser-assisted particle combustion experimental setup	61
3.27 The burn time- particle size correlation for combustion in air of the prepared B-milled oxidizer samples	62

CHAPTER 1

INTRODUCTION

There are plethora of milling processes which are vastly used for grinding materials into fine powders, preparation of oxidizers and mechanochemistry. Ball milling is one amongst them. Different types of mills used include, most commonly, shaker, planetary, and attritor mills. There are various parameters involved in ball milling process which includes ball-to-powder mass ratio (BPR), milling media material and size, powder charge per vial, milling time, as well as type and amount of the used process control agent (PCA). Each process parameter may have a crucial effect on the characteristics of the produced milled powders. Among many such characteristics, particle size distribution, surface morphology and crystallinity are commonly important for applications.

Previous work showed that BPR has a significant effect on the time required for achieving steady state/particular phase in ball milling.¹ A higher BPR generally translates into higher milling energy. Respectively, to maintain the desired total energy transferred to the powder from milling media, milling time may need to be reduced with an increase in BPR.² The size and type of milling media also has an effect on the surface morphology. Using different milling media like stainless steel balls, and zirconium balls show different effect due to different thermal conductivities and specific gravities.³ In the past, effects of BPR, milling time, and agitation intensity, often expressed through RPM for planetary and attritor mills, were combined to consider milling dose, quantifying the overall energy transfer to the powders being processed⁴⁻⁸.

Most of previous research focused on milling parameters, which are relatively easy to quantify and express in terms of their effect on the milling energy. Less clear are effects

of PCAs, which nonetheless can be very important for the properties of the product obtained during milling. It is known, for example, that PCAs have an effect on agglomeration and deagglomeration of the powder particles^{9, 10}. In addition to cold welding that may affect the particle size and milling effectiveness, powders might be caking in the milling vials, attaching to the walls; these processes are routinely managed using PCA. For example, to limit cold welding and minimize caking, PCAs having a lubricating effect are used.¹¹ Employing different PCAs will lead to different yield during milling process. PCA may also affect the crystallite boundaries of the powders during the milling process. However, the effect of PCA is not well understood and there are no models correlating the properties of PCA with characteristics of the produced powders.

In the first part of this thesis, a systematic experimental study is described that compares the effects of a broad range of fluids serving as PCA on properties of the milled oxide powders. Specifically, oxides of copper and bismuth were selected for the experiments. These are oxides commonly used as oxidizers in various thermite compositions. In the present experiments, effect of different PCAs used to ball mill Bi_2O_3 and CuO powders was considered focusing on the powder particle size and crystallinity obtained after ball milling. The effect of multiple physical and chemical PCA properties on the characteristics of the milled powder was analyzed based on the experimental data. In the second part of this research, the experimental work focusing on the effect of PCA on properties of milled powder was followed up by using these powders to prepare novel thermites with binary oxidizers, combining the two oxides. Individually, metal oxides, including CuO and Bi_2O_3 , have been used as oxidizers for various purposes including chemical looping combustion¹² and catalytic oxidation reactions¹³ in various chemical

engineering fields. They are also used in thermites, serving as components of reactive materials ^{14, 15, 16}. Recently, it was suggested that binary oxides of CuO and Bi₂O₃ may be advantageous for performance of boron-based thermites ¹⁷. Specifically, it was shown that thermites with binary oxidizers ignited at a lower temperature compared to those using individual oxides¹⁷.

However, the oxides were only mixed as individual nanopowders. Preparation of binary oxidizers, mixed mechanochemically or synthesized together was expected to enrich our understanding of the synergistic effects of different individual oxidizers. Such effects have not been studied. In this work, fuel-rich thermite system were of interest, capable of combusting effectively in an oxidizing environment ^{18, 19}. Generally, mixed oxides having lower decomposition temperatures will have a significant effect in ignition at higher heating rates. Oxidation, ignition, and combustion of the prepared powders were studied in this effort. Directions for the future research implied by the present results are discussed for both parts of this effort.

CHAPTER 2

EFFECT OF SOLVENT USED AS PROCESS CONTROL AGENT ON PROPERTIES OF BALL MILLED POWDERS

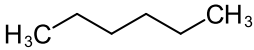
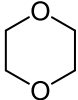
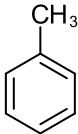
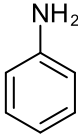
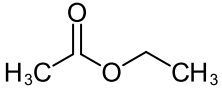
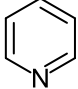
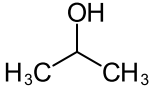
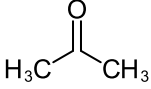
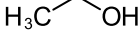
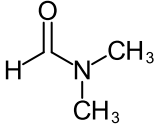
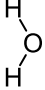
2.1 Experimental

2.1.1 Material and Material Preparation

Powders of bismuth (III) oxide (99% pure) from Alfa Aesar and copper (II) oxide (98% pure) from Sigma Aldrich were used. Table 1 shows the organic solvents used, their chemical formula and molecular structure along with their suppliers.

Each oxide powder was milled for 20 min in a SPEX Certiprep 8000 series shaker mill using 9.25-mm diameter steel balls as milling media and 7 mL of PCA. Each of the 13 solvents listed in Table 1 served as PCA in different runs. The powder charge per milling vial was 5 g and the ball-to-powder ratio (BPR) was fixed at 10. The milled powders were recovered as a slurry and dried in ambient lab air. They were stored dry for the duration of the experiments.

Table 2.1 Chemical Formula, Molecular Structure of the Solvents used in this Study

Solvent	Chemical formula	Molecular sketch	Purity, %	Supplier
Hexane	C_6H_{14}		98.5	Millipore/MercK
1,4-Dioxane	$C_4H_8O_2$		99.8	Alfa Aesar
Toluene	C_7H_8		95	Kleanstrip
Aniline	$C_6H_5NH_2$		99	Alfa Aesar
Ethyl Acetate	$C_4H_8O_2$		99.5	VWR International
Pyridine	C_5H_5N		99.5	Alfa Aesar
Isopropyl Alcohol	C_3H_8O			
Acetone	C_3H_6O		99.5	Sunnyside
Ethanol	C_2H_5OH		95	Carolina
Methanol	CH_3OH	H_3C-OH	99.9	Sigma Aldrich
N,N-Dimethyl Formamide	C_3H_7NO		99.8	Alfa Aesar
Acetonitrile	C_2H_3N	$H_3C-C\equiv N$	99.9	J.T. Baker
Water	H_2O		~	

2.1.2 Material Characterization

The milled powders were characterized by X-ray diffraction (XRD) on a PANalytical Empyrean multipurpose research diffractometer for compositional analysis and crystallite properties. The diffractometer was operated at 45 kV and 40 mA using Cu K α radiation ($\lambda = 1.5438 \text{ \AA}$).

The size distribution of the milled powders was analyzed on Malvern Mastersizer 3000. The instrument was operated using a Hydro MV dispersion unit with 80 % sonication intensity. The speed of the impeller was maintained at 2250 RPM to avoid the agglomeration and settling of particles. Milli-Q water was used as a powder dispersant. The powder was added until a 5-8% obscuration was achieved

2.2 Results

2.2.1 Compositional Analysis and Crystallite Properties

The XRD patterns of bismuth oxide milled in different solvents are presented in Figure 2.1. The topmost plot is that of the un-milled bismuth oxide provided for reference. Peak broadening occurs for all the milled samples. For the bismuth oxide milled in methanol, ethanol, acetone, and isopropyl alcohol, some unidentified peaks are observed. These peaks suggest that a chemical reaction occurred between bismuth oxide and the PCA.

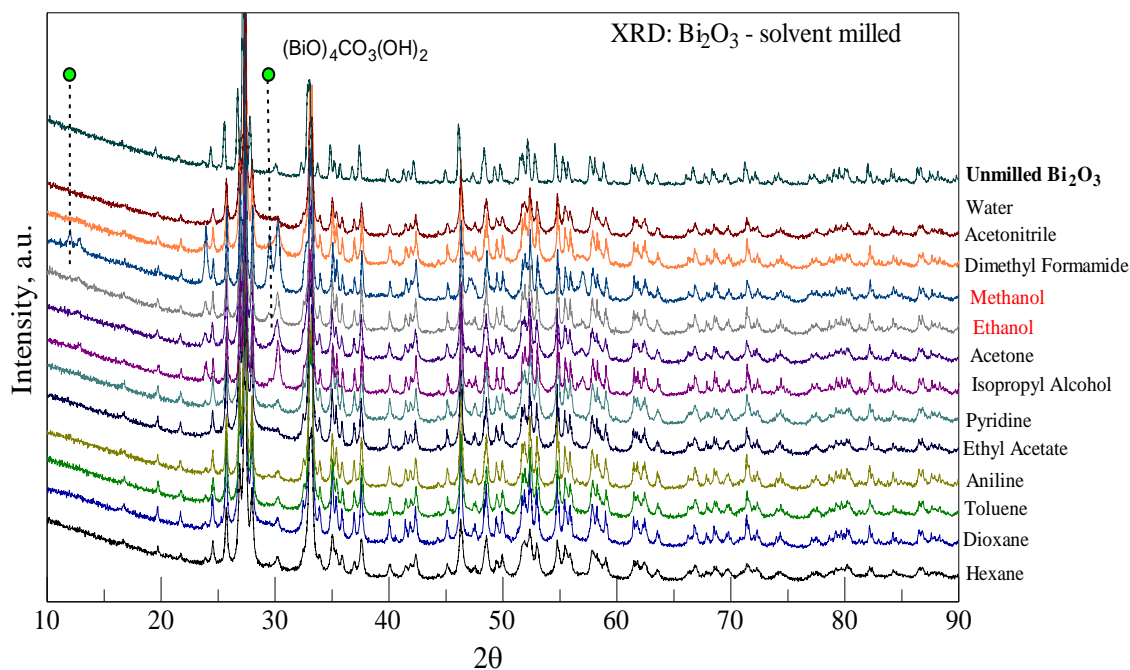


Figure 2.1 XRD traces of freshly milled powders of bismuth (III) oxide milled in different solvents under identical conditions. The solvents used as PCA are listed beside their respective trace.

Similarly, the XRD traces of copper oxide milled with different PCAs are presented in Figure 2.2. The first trace belongs to unmilled copper oxide. All milled powders are comparable to reference copper oxide. For the copper oxide milled in acetone, a minor unidentified peak was observed at $\sim 27^\circ$ suggesting a possible chemical reaction.

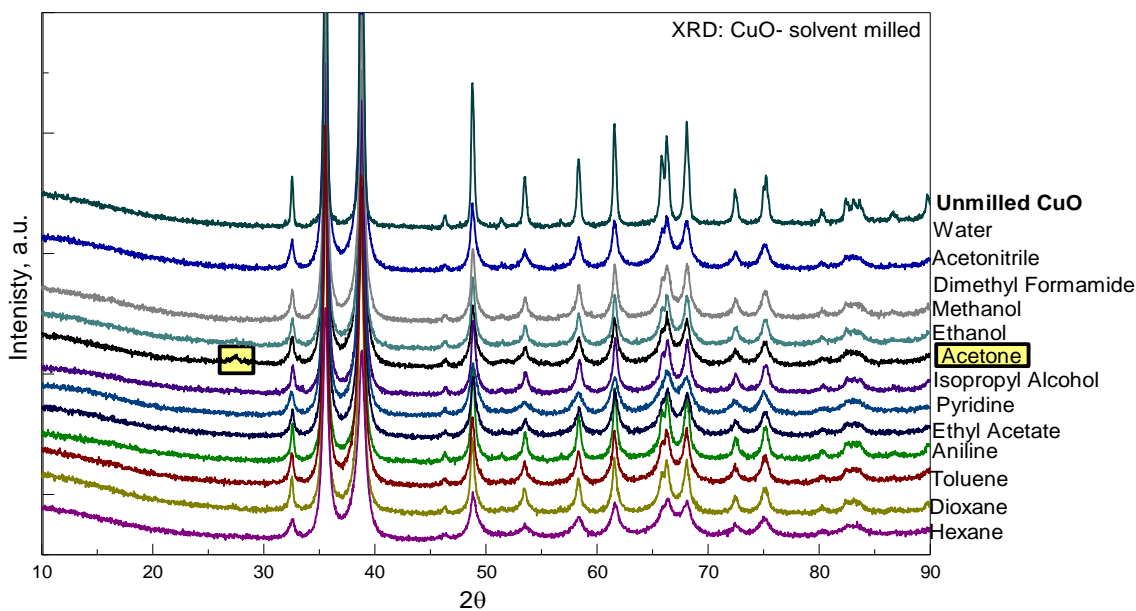


Figure 2.2 XRD traces of freshly milled powders of copper (II) oxide milled in different solvents under identical conditions. The solvents used as PCA are listed beside their respective traces.

2.2.2 Particle Size Distribution (PSD) Analysis

The bulk physical properties of the milled powders were followed to quantify the effect of PCA on the powders. Towards this end, the particle size distribution of both the oxide powders was obtained to identify solvents that yielded favorable small-sized particles.

Figure 2.3 represents the particle size distributions for all the bismuth oxide milled with different solvents. Un-milled bismuth oxide is shown as a reference in all the particle size distribution graphs with different solvents.

As seen in Figure 2.3, all bismuth oxide samples show bi-modal characteristics unlike the starting material. Most of the bismuth oxide milled powders lie in the range of 0.2 μm to 50 μm . However, in the case of bismuth oxide milled in methanol, it shows the tri-modal characteristics with the particle size varying between 0.2 μm and 650 μm . The

particle size distributions for different solvents are distinct when compared with an un-milled bismuth oxide size distribution plot.

Figure 2.4 presents the particle size distribution of copper oxide powders milled in different solvents under identical conditions as bismuth oxide. Un-milled copper oxide is plotted as reference with the plots for different solvents. Most of the size distributions are asymmetric with a long tail towards smaller sizes. The samples largely lie in the vicinity of 5 μm and 12 μm except for copper oxide milled in aniline. This sample was observed visually to be gritty and large. It can be observed that particle size distribution for reference (un-milled) copper oxide is almost identical to most of the solvents.

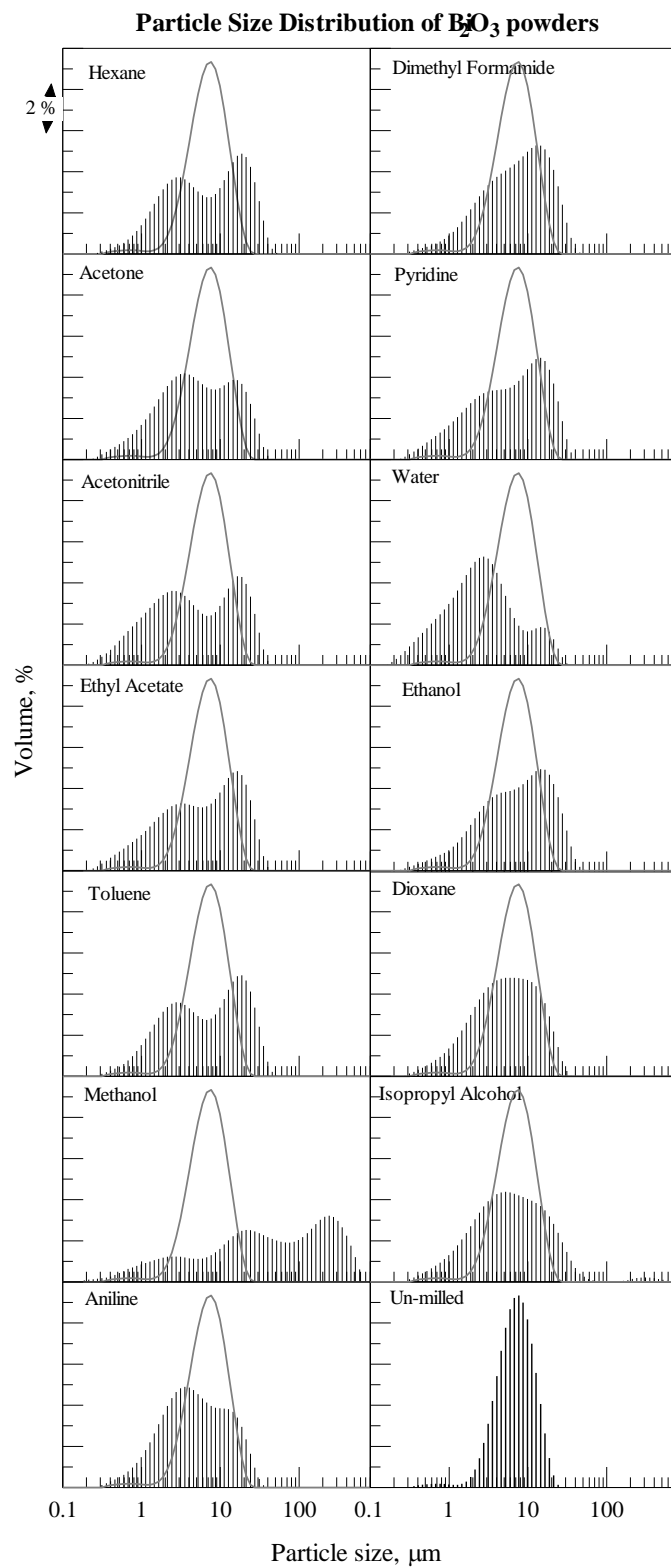


Figure 2.3 The particle size distribution of bismuth (III) oxide powders milled in different solvents under identical conditions.

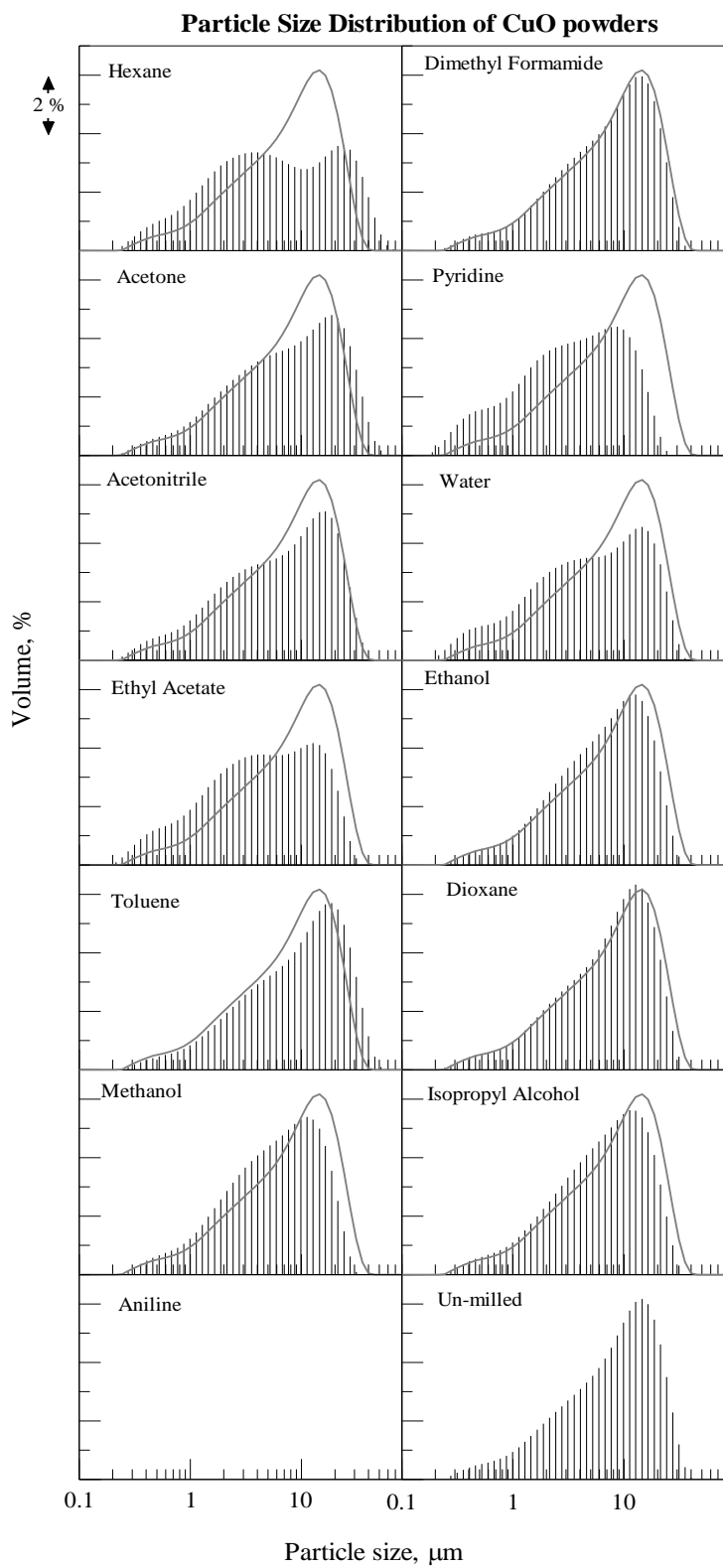


Figure 2.4 The particle size distribution of copper (II) oxide powders milled in different solvents under identical conditions.

2.3 Discussion

2.3.1 Correlation between Solvent Properties and Milled Powder Properties

To establish systematic relationships between the results of milling and properties of the used PCAs, the obtained data set was explored for systematic correlations. A preliminary principal component analysis showed that different particle size descriptors such as the volume moment mean $D[4,3]$ or the Sauter mean diameter $D[3,2]$ were highly correlated with each other. For this reason, a single descriptor, the surface area median diameter, D_{50} , was used to represent the particle size measurements. The XRD measurements were represented by the obtained crystallite size. Table 2.2 summarizes these values for both sets of powders. Properties of the PCAs are listed in Table 2.3. The specific properties used for correlation analysis, marked in Table 2.3, are dynamic viscosity, dielectric constant, dipole moment, density, proton affinity, surface tension, and enthalpy of vaporization.

Table 2.2 The Crystallite Size and Surface Area based Bulk Powder Property (D_{50}) of Milled Bi_2O_3 and CuO Powders Obtained by Milling in Various Solvents Employed as Process Control Agents under Identical Conditions.

PCA used	Milled Bi_2O_3		Milled CuO	
	Crystallite size	D_{x50} (Surface area)	Crystallite size	D_{x50} (Surface area)
Hexane	476.9	1.81	238.2	1.13
1,4-Dioxane	804.7	2.06	386.4	1.76
Toluene	780.1	1.73	303.9	1.92
Aniline	721	1.91	412.2	
Ethyl Acetate	711.7	1.24	279.9	1
Pyridine	777	1.38	377.6	0.802
Isopropyl Alcohol	1749.5	1.82	321.5	1.75
Acetone	799	1.52	296.7	1.51
Ethanol	1039.5	1.9	326	1.88
Methanol	1307.4*	1.04*	313.6	1.71
N,N-Dimethyl Formamide	845	2.3		1.67
Acetonitrile	507.5	1.1	319.3	1.3
Water		0.884*	265	0.935

* indicates outliers

With two milling outcomes, and two materials, a total of four data sets were analyzed. The milling outcomes will be referred to as M_i , where $i = (1 \dots 4)$, indicates a specific combination of milling outcome and oxide. Bismuth oxide shows signs of chemical alteration after milling with methanol or water (see Figure 2.1). These data points were therefore not used for this correlation analysis.

To examine possible effects on the milling outcome of $n=7$ different characteristics ζ of the PCAs shown in Table 2.3, each outcome was described by a linear model of the form:

$$\log(M_i) = \log(M_i^0) + \sum_{j=1}^n a_j \zeta_j \quad (1)$$

where the intercept $\log(M_i^0)$ and the coefficients a_i were determined by multivariate least-squares fitting. Each such model is characterized by $(n+1)$ adjustable parameters.

Table 2.3 Properties of the PCAs Used in this Study

PCA used	Boiling point, °C	Dynamic Viscosity, cP [†]	Polarity index	Dielectric constant [†]	Dipole moment, Cm [†]	Density, g/mL [†]	Proton affinity, kJ/mL [†]	Surface tension, mN/m [†]	Enthalpy of vaporization, kJ/mL [†]
Hexane (C ₆ H ₁₄)	68.7	0.31	0.1	1.88	0.08	0.659	5.174	18.43	0.241
1,4-Dioxane (C ₄ H ₈ O ₂)	101.3	1.44	4.8	2.25	0.45	1.033	9.348	33	0.452
Toluene (C ₇ H ₈)	110.6	0.59	2.4	2.38	0.31	0.865	7.360	28	0.356
Aniline (C ₆ H ₅ NH ₂)	131.7	0.8	2.7	5.62	5.2	1.0297	9.757	43.4	0.617
Ethyl Acetate (C ₄ H ₈ O ₂)	77.1	0.46	4.4	6.02	1.88	0.902	8.555	23	0.358
Pyridine (C ₅ H ₅ N)	115.2	0.95	5.3	12.4	2.37	0.978	11.498	38	0.496

Isopropyl Alcohol (C ₃ H ₈ O)	82.3	2.4	3.9	19.92	1.66	0.7854	10.363	22	0.593
Acetone (C ₃ H ₆ O)	56.3	0.32	5.1	20.7	2.69	0.791	11.058	25.2	0.426
Ethyl Alcohol (C ₂ H ₅ OH)	78.3	1.1	-	24.55	1.66	0.789	13.296	22.1	0.726
Methanol (CH ₃ OH)	64.7	0.59	5.1	32.7	2.87	0.791	18.622	22.7	0.933
N,N-Dimethyl Formamide (C ₃ H ₇ NO)	153	0.92	6.4	36.71	3.86	0.948	11.511	37.1	0.608
Acetonitrile (C ₂ H ₃ N)	81.6	0.37	5.8	37.5	3.44	0.786	14.919	27.54	0.632
Water (H ₂ O)	100	1	10.2	80.1	1.87	1	38.356	72.86	2.441

†used for correlation analysis

For each milling outcome, $(n+1)$ -parameter models with all possible $2^7 = 128$ combinations of parameters, including the case for $n = 0$ were fitted to the data, and the results were evaluated in terms of the logarithmic likelihood of the obtained fit. The trade-off between the model likelihood and the numbers of parameters used was evaluated using the Akaike information criterion modified for small sample sizes, AIC_C. The model with the lowest AIC_C value is considered the most prudent, achieving the best fit while using the fewest adjustable parameters.

Selected results are shown in Table 2.4 for Bi₂O₃, and Table 2.5 for CuO. Each line in these tables lists the coefficients of a linear model of the form shown in Eq. (1).

Blank cells indicate that the respective PCA property and corresponding coefficient a were not used. The last two columns show the log likelihood function, and $\delta\text{-AIC}_C = (\text{AIC}_C - \min(\text{AIC}_C))$

The results are graphically presented in Figures 2.5 and 2.6 for experiments with Bi_2O_3 and CuO , respectively. The figures show the obtained log-likelihood vs. $\delta\text{-AIC}_C$ for all models. Figures 2.5 (a) and 2.6 (a) show the cases of surface area based median particle size, while Figures 2.5 (b) and 2.6 (b) show the case of the crystallite size. In these figures, the models form groups, apparent as straight lines, corresponding to how many adjustable parameters were used in a model. Each such group shows the model with the highest log-likelihood at the left end, indicated by arrows.

Table 2.4 Coefficients of Linear Models Describing Measured Results as Function of PCA Properties for Bi₂O₃

Intercept	Dielectric constant	Density	Dipole moment	Enthalpy of vaporization	Proton affinity	Surface tension	Dynamic viscosity	Log Lik	δ-AIC _c
Coefficients for surface area based median particle size									
0.37533							0.156	2.47	1.670
0.6947				1.9290	-0.111			5.84	0.165
0.8638	0.006			1.942	-0.138			6.46	6.259
0.5614	0.010	0.495		1.771	-0.148			7.17	15.83
0.56135	0.012		-0.09	1.997	-0.147	0.016		9.61	29.29
Coefficients for crystallite size									
6.2506							0.479	4.20	0
6.2140	0.002						0.476	4.42	4.812
6.4219			0.045			-0.009	0.496	4.99	11.00
6.40533			0.041	0.049		-0.009	0.490	4.99	22.00
6.08960		0.725	0.058		0.0009	-0.020	0.477	5.31	39.70

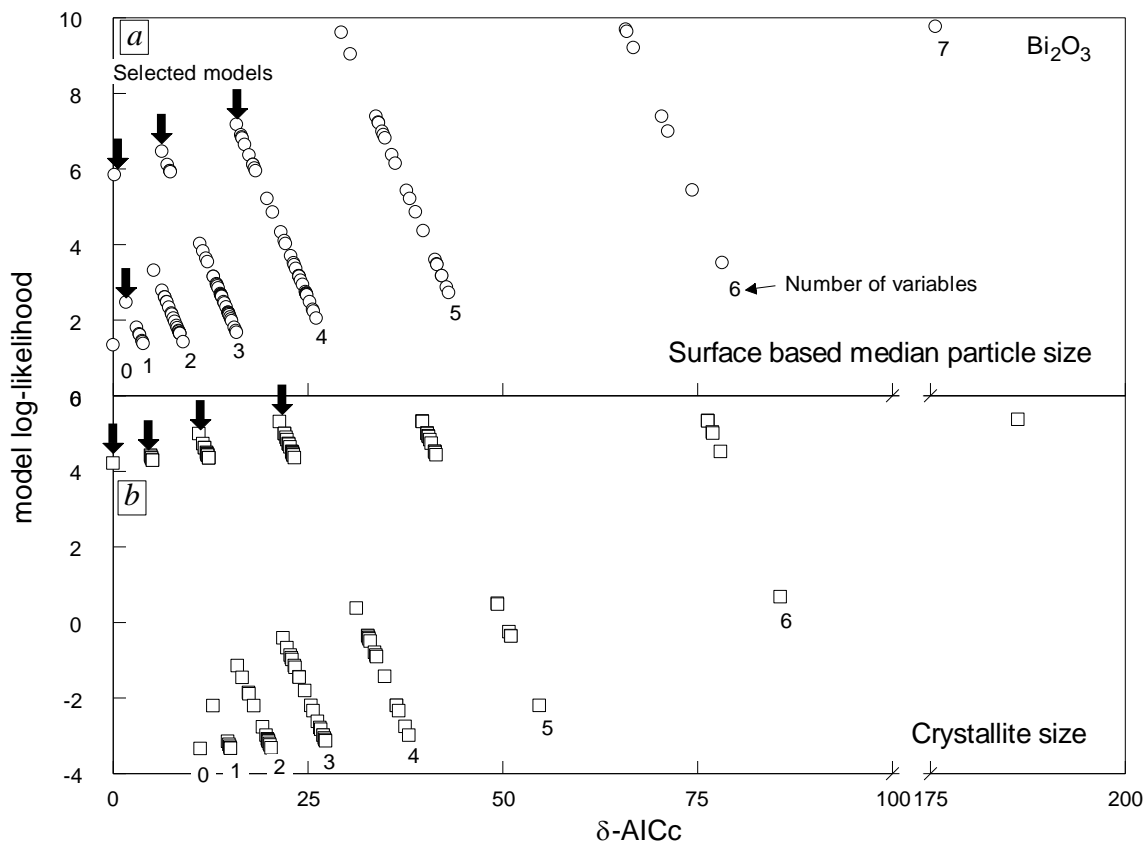


Figure 2.5 Correlation between log-likelihood and δ -AICc values for Bi_2O_3 powder based on (a) surface based median particle size and (b) crystallite size.

Table 2.5 Coefficients of Linear Models Describing Measured Results as Function of PCA Properties for CuO

Intercept	Dielectric constant	Density	Dipole moment	Enthalpy of vaporization	Proton affinity	Surface tension	Dynamic viscosity	Log Lik	δ -AICc
Coefficients for surface area based median particle size									
0.61						-0.009		-0.85	1.09
0.48						-0.009	0.165	-0.00	4.11
0.54	0.004					-0.014	0.171	0.39	9.59
-0.73	0.023	2.768	-0.186			-0.048		1.95	15.2
-1.17	0.059	3.975	-0.432	-1.208		-0.052		4.34	23.70
Coefficients for crystallite size									
5.05		0.804						8.44	0.78
4.74		1.417				-0.007		11.1	0
4.76		1.316	0.040			-0.007		13.5	1.61
4.78		1.184	0.047			-0.007	0.075	15.4	6.56
4.91		0.810	0.045	-0.395	0.0171		0.111	16.3	17.8

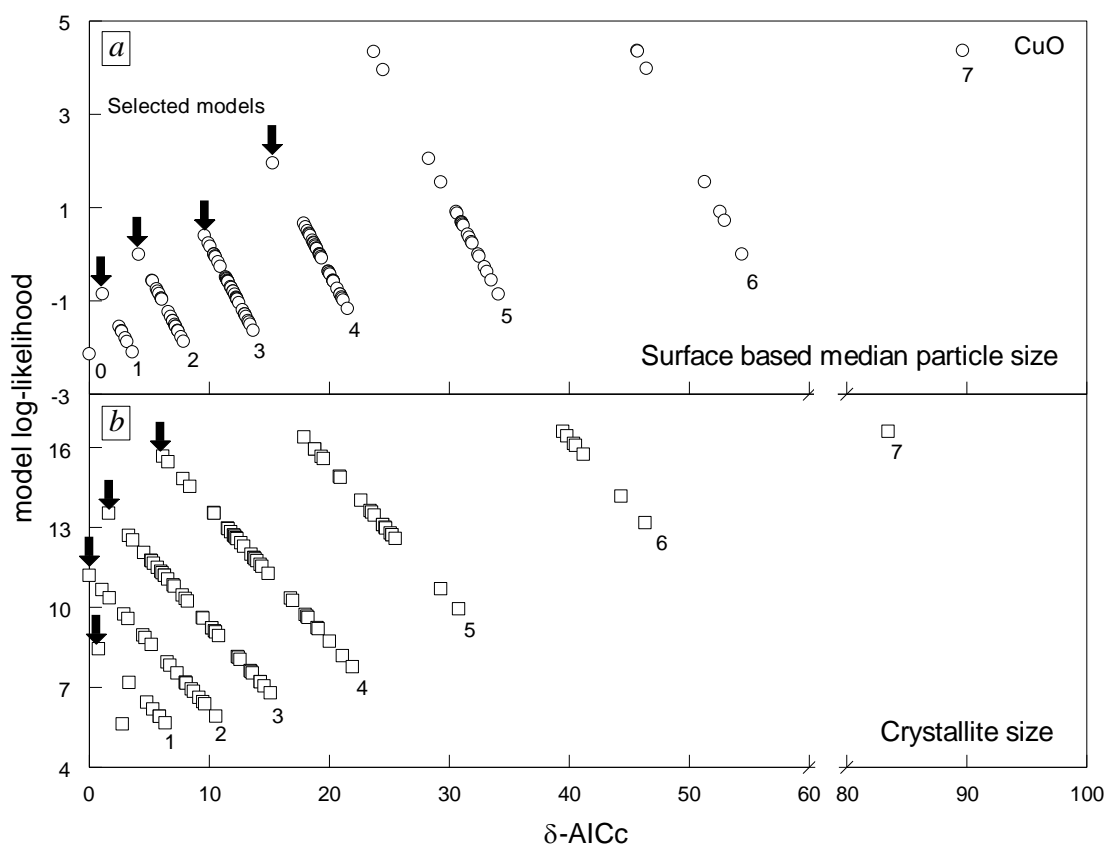


Figure 2.6 Correlation between log-likelihood and δ -AICc values for CuO powder based on (a) surface based median particle size and (b) crystallite size.

Due to the relatively small size of the data set, and no a-priori assumption about how PCA properties should affect the milling outcomes, the outcomes (D_{50} and crystallite size for Bi_2O_3 and CuO) were calculated using the respective models with highest log-likelihood, and compared to the observed experimental results. This is shown in Figure 2.7 for Bi_2O_3 and Figure 2.8 for CuO. In each figure, the results are shown in order of increasing experimentally observed particle size or crystallite size, respectively.

For the surface area based median particle size of Bi_2O_3 (Figure 2.7 (A)), all the linear models with the highest log-likelihood appear to reproduce the experimental results

equally well, regardless of the number of parameters used. The PCAs Acetone and DMF appear as outliers, not described by any of the linear models within their standard errors.

For the crystallite size of Bi_2O_3 (Figure 2.7 (B)), the predictions of the models are again similar, regardless of the number of parameters used. Here, acetone is also not well described, although DMF falls within the standard error of all models shown.

The predictions for the surface area based median particle size of CuO (Figure 2.8 (A)) differ according to the number of parameters used. The 3-parameter model, using two PCA properties, specifically surface tension and dynamic viscosity (see Table 5), predicts values for D_{50} that overlap for most PCAs, and does not reproduce the observed experimental trend. In contrast, the model using 6 adjustable parameters, or five PCA properties, does adequately reproduce most experimental results with ethyl acetate and toluene as outliers.

The models for the crystallite size of CuO (Figure 2.8 (B)) all reproduce the observed results equally well regardless of number of parameters used. Ethyl acetate and ethanol are notable outliers.

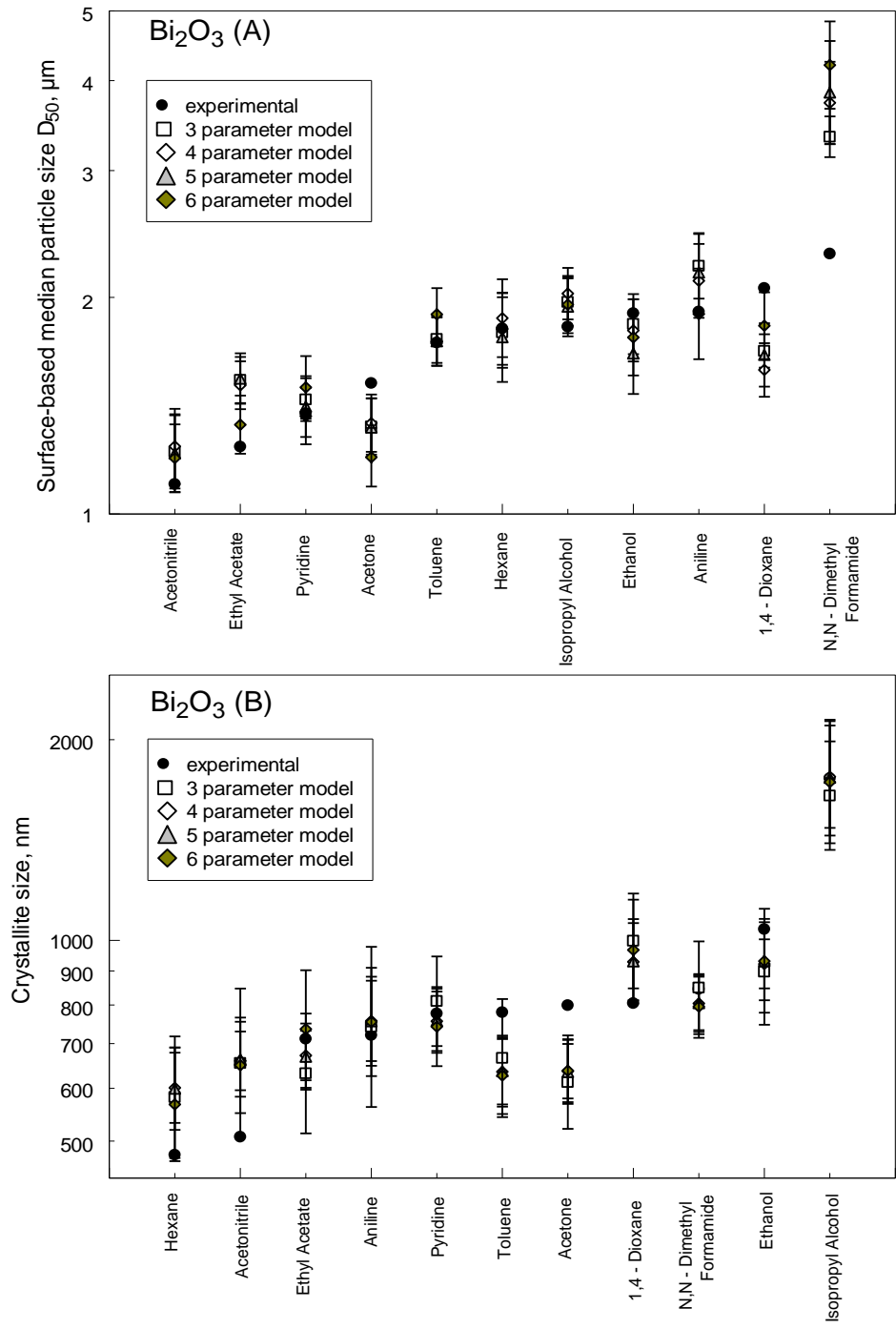


Figure 2.7 Observed and predicted milling outcomes of (A) surface based particle size and (B) crystallite size for Bi₂O₃.

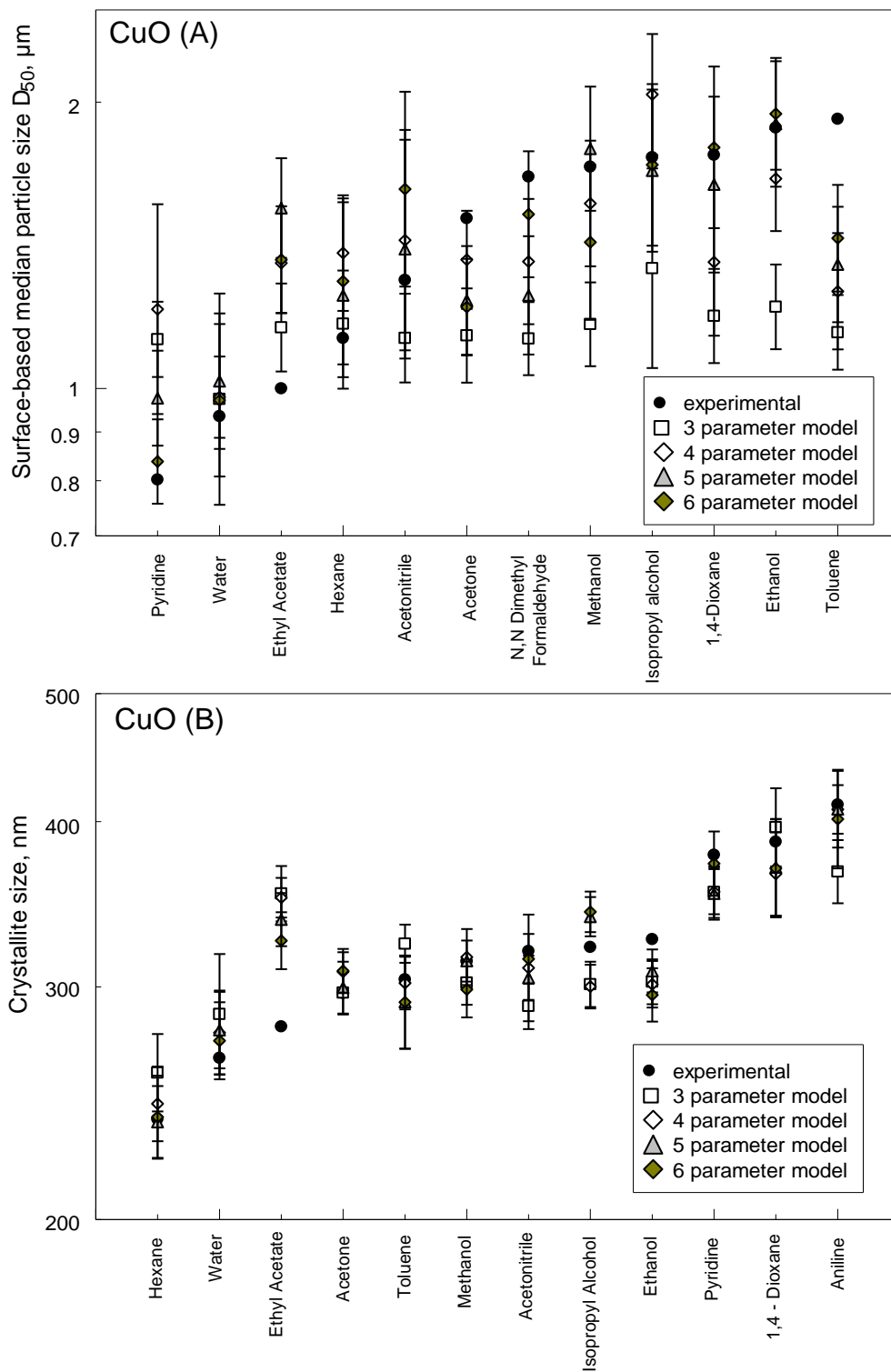


Figure 2.8 Observed and predicted milling outcomes of (A) surface based particle size and (B) crystallite size for CuO.

CHAPTER 3

EFFECT OF $\text{Bi}_2\text{O}_3\cdot\text{CuO}$ BINARY OXIDIZER ON BORON'S IGNITION AND COMBUSTION IN FUEL-RICH COMPOSITION

3.1 Experimental

3.1.1 Experimental Approach

Binary oxidizers were prepared by two methods. The first method involved ball-milling commercially sourced oxide powders to produce milled binary oxidizers. These binary oxides are referred to as “milled”. The second method involved thermal decomposition of finely mixed nitrates and calcining the formed oxides of bismuth and copper to synthesize binary oxidizers. These oxides are referred to as “synthesized”.

Five target compositions were prepared by both methods as shown in Table 3.1. Prepared by increasing Bi_2O_3 concentration in 25 wt. % steps, from pure CuO to pure Bi_2O_3 , the oxidizers included three binary compositions and two reference end-members: CuO and Bi_2O_3 .

Table 3.1 Targeted Oxidizer Compositions and their Nomenclature

Composition No.	Oxidizer Nomenclature	Bi_2O_3 in Oxidizer	
		Mass, %	Mole, %
1	100CuO (reference)	0	0
2	25 $\text{Bi}_2\text{O}_3\cdot$ 75CuO	25	5.4
3	50 $\text{Bi}_2\text{O}_3\cdot$ 50CuO	50	14.6
4	75 $\text{Bi}_2\text{O}_3\cdot$ 25CuO	75	33.9
5	100 Bi_2O_3 (reference)	100	100

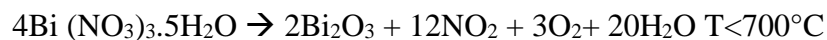
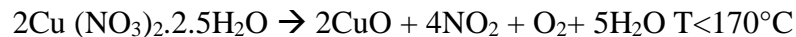
The obtained oxidizers were then added to boron to prepare composites by arrested reactive milling (ARM). To ensure comparability across different preparation techniques

and oxidizer compositions, the equivalence ratio of boron to added oxidizer was kept constant. The prepared boron-oxidizer samples were subsequently characterized and tested for their oxidation, ignition and combustion behaviors.

3.1.2 Preparation of Oxidizers

The preparation of milled oxidizers involved the milling of bismuth (III) oxide (99% pure) sourced from Alfa Aesar and copper (II) oxide (98% pure) from Sigma Aldrich in a SPEX Certiprep 8000 series shaker mill. A total charge of 5 g was milled with fourteen 9.25-mm steel balls (50.8 g) which translates to a ball-to-powder mass ratio (BPR) of 10. The mass of Bi₂O₃ in the charge was changed to achieve the targeted compositions presented in Table 3.2. The oxide powders were milled in steel milling vials sealed in air for 30 min without any process control agent (PCA). The reference oxide powders were prepared by replicating the milling protocol using pure CuO and Bi₂O₃. All the prepared milled oxidizers have size distributions with similar characteristics; positive skewed distributions, spanning from 0.2 μm to 50 μm, with a mode in the vicinity of 10-20 μm can be observed in Figure 3.1 (A).

The preparation of synthesized binary oxidizers involved thermally decomposing the finely mixed hydrated nitrates of bismuth and copper and calcining the resulting oxides, in air. The equations below describe the temperature dependent decomposition reactions:



Bismuth (III) nitrate pentahydrate (98% pure) sourced from Beantown Chemical and copper (II) nitrate hemi(pentahydrate) (99% pure) sourced from Alfa Aesar were ground together using a mortar and pestle, to form a homogenous mixture. The total mass of the initial nitrate(s) powder depended on the composition and was adjusted such that 12 g of oxide(s) powder was obtained at the end of the heating program. The mass of nitrates taken to obtain the oxidizer compositions is summarized in Table 3.2.

Table 3.2 Targeted Synthesized Oxidizer Compositions and the Required Mass of their Corresponding Nitrates to obtain 12g of Oxidizer.

12g Synthesized Oxidizer	Bi ₂ O ₃ in Oxidizer	CuO in Oxidizer	Bi (NO ₃) ₃ · 5H ₂ O	Cu (NO ₃) ₂ · 2.5H ₂ O	Total Nitrate
	Mass, g	Mass, g	Mass, g	Mass, g	Mass, g
100CuO (reference)	0	12	0	35.09	35.09
25Bi ₂ O ₃ ·75CuO	3	9	6.25	26.32	32.56
50Bi ₂ O ₃ ·50CuO	6	6	12.49	17.54	30.04
75Bi ₂ O ₃ ·25CuO	9	3	18.74	8.77	27.51
100Bi ₂ O ₃ (reference)	12	0	24.98	0	24.98

The ground nitrate powders were placed in a 60 mL closed alumina crucible and heated in a bench top oven in air. The powders were heated at 5 K/min from room temperature (~25 °C) to 850 °C in three stages. The powders were first heated to 170 °C and isothermally held for 2 hours to complete decomposition of hydrated copper nitrate into copper (II) oxide. Subsequently the powder was heated to 700 °C and held for 2 hours to conclude the decomposition of hydrated bismuth nitrate into bismuth (III) oxide. The powders were further heated beyond the melting point of Bi₂O₃ (820°C) to 850°C and held for 20 min before cooling to room temperature. A portion of the dense molten Bi₂O₃ sunk

to the bottom and fused with the alumina crucible. This loss of Bi_2O_3 to the crucible during synthesis yielded binary-oxidizers with increased CuO mass fraction.

To address this shortcoming, an alternative two stage heating program was employed to prepare Bi_2O_3 -rich binary- oxidizer, $75\text{Bi}_2\text{O}_3 \cdot 25\text{CuO}$. The nitrate powder was heated at 1 K/min with two isothermal stages at 170 °C and 700 °C, each 2 hour-long. The temperature remained below the melting point of Bi_2O_3 . The cooled powder obtained at the end of the run was ground using a mortar and pestle and re-heated using the same heating program. This cycle was repeated two more times to ensure formation of a homogenous binary-oxidizer.

The synthesized oxidizer powders obtained after heat treatment were very coarse. All the oxidizers except CuO, exhibit a bimodal distribution peaking in the ranges 20-100 μm and 100-1000 μm which can be observed in Figure 3.1 (B). CuO size distribution was log-normal with a peak in the vicinity of 40 μm .

To reduce particle sizes, all synthesized oxidizer powders were ball-milled in excess liquid PCA for 60 min. A charge of 5 g was milled in the shaker mill with 14 mL hexane as PCA. Steel balls of 5 mm size were employed as milling media while the BPR was fixed at 10. The resulting powders were air-dried and stored for subsequent characterization prior to milling them with boron. The size distributions of these milled synthesized powders were comparable to one another across compositions with an average size of $\sim 8 \mu\text{m}$ can be observed in Figure 3.1 (C). Both sets of prepared oxidizers were stored in air until they were milled with boron.

3.1.3 Preparation of Boron-Oxidizer Reactive Powders

Reactive composites were prepared using 95 % pure amorphous boron sourced from SB Boron. The as received boron was first de-agglomerated by ball milling. A charge of 5 g of boron per steel vial was milled in the shaker mill for 60 min. Fourteen 9.25-mm steel balls per vial were used as milling media to achieve a BPR of 10. Hexane (0.8mL) was used as the PCA in each vial.

The de-agglomerated boron was then milled with the prepared set of oxidizers by ARM. The mass of boron per milling vial was fixed at 2.5 g while the mass of the oxidizer was dependent on its composition to ensure a boron-to-oxygen molar ratio of 14.4 across all reactive composites prepared. This translated to an equivalence ratio of 21.6, calculated by considering the reaction between boron and the added oxidizer; $B + xBi_2O_3 \cdot (100-x)CuO$. Table 3.3 presents the targeted compositions of the boron-binary oxidizer reactive composites along with the reference single oxide-containing reactive powders.

The targeted compositions seen in Table 3.3 were used for boron-milled oxidizer powders. The boron-synthesized oxidizers on the other hand had less than targeted Bi_2O_3 and hence boron mass was corrected based on compositional analysis of the synthesized oxidizers.

The powders of boron and milled oxidizers were milled with 9.25-mm steel balls. The powders of boron and synthesized oxidizers were milled with 5-mm steel balls. In all cases, BPR was 10 and 8 mL of hexane served as PCA. The vials were sealed in an argon-filled glove box and milled for 60 min in the shaker mill.

Table 3.3 Targeted Composition of Boron-Oxidizer Samples

Composition	Mass, %			Equivalence Ratio
	Boron	Bi ₂ O ₃	CuO	
B·100CuO (reference)	66.1	0	33.9	21.6
B·25Bi ₂ O ₃ ·75CuO	63.2	9.2	27.6	
B·50Bi ₂ O ₃ ·50CuO	59.6	20.2	20.2	
B·75Bi ₂ O ₃ ·25CuO	55.3	33.5	11.2	
B·100Bi ₂ O ₃ (reference)	50.0	50.0	0	

The obtained reactive samples were passivated in an argon-filled glovebox where air was present at a low partial pressure for 24 hours. Passivated powders were stored under hexanes for the duration of experimentation.

3.1.4 Material Characterization

The prepared oxidizer powders and reactive composites were characterized for their chemical composition using X-ray diffraction (XRD) on a PANalytical Empyrean multipurpose research diffractometer operated at 45 kV and 40 mA using filtered Cu K α radiation. The size distribution of the prepared oxidizers as well as reactive composites was examined by laser diffraction on a Malvern Mastersizer 3000 operated using the Hydro MV dispersion unit. The Hydro MV unit was operated at 80 % sonication intensity, with an impeller speed of 2250 RPM to prevent agglomeration of particles. The powders were dispersed in Milli-Q water until an obscuration value in the range of 5-8% was achieved to obtain size distributions.

The boron-binary oxidizer reactive powders were examined using a JEOL JSM-7900 emission scanning microscope (SEM). Back-scattered electrons were used to obtain

phase contrast to distinguish oxidizer from boron. Where necessary, energy dispersive X-ray spectroscopy (EDX) was used to discern compositional detail.

The reactivity of the prepared powders was characterized by thermogravimetric analysis (TGA) coupled with either differential scanning calorimetry (DSC) or differential thermal analysis (DTA) on a Netzsch Thermal Analyzer STA409PG. Based on the experimental setup, alumina DTA or DSC crucibles were employed. Small sample mass of 5 ± 1 mg was heated at 5 K/min in oxidative and inert atmospheres. Separate inert runs were performed in DTA setup with higher sample masses (32 ± 1 mg) at a higher heating rate of 40 K/min for improved resolution. The temperature program began at 25 °C and extended to 700 °C for all samples heated at 5 K/min and to 800 °C for samples heated at 40 K/min. The inert environment was sustained by flowing ultra-pure argon (99.998 % pure) at 50 mL/min. The oxidative atmosphere was achieved by an additional oxygen (99.994 % pure) stream flown at 50 mL/min. Both gases were obtained from Airgas. The spent samples at the end of both oxidative and inert runs were collected and analyzed by XRD to identify compositional changes.

3.1.5 Heated Filament Experiment

The ignition temperature of milled reactive powders was obtained by electrically heating the sample at the rates in the range of 10^3 - 10^4 K/s. As the sample coated on a nickel-chromium filament was heated, the wire's intensity and the powder emission were temporally followed using a calibrated photodiode and high-speed video camera. The experimental setup and procedure are described in detail elsewhere^{20, 21}. A thin coat of powder in the form of a hexane slurry was applied onto a nickel-chromium filament of 1-mm diameter. Once the solvent dried off, the filament was electrically heated using a

variable set of rechargeable large cell 7238K57 McMaster Carr batteries and a custom-built 1- Ω rheostat connected in series. An optic fiber was focused on an uncoated section of the wire and fed into a germanium photo diode, PDA30B2 by Thorlabs. The photodiode served as a pyrometer as it was calibrated against a black body emission source, BB4A by Omega engineering. The ignition instant identified using a high-speed video taken by a MotionPro 500 camera by Redlake. That instant was correlated with the temperature of the wire measured by the pyrometer simultaneously. At least 8 runs were performed for each targeted heating rate.

3.1.6 Particle Combustion Experiments

The particle combustion experiment was conducted by aerosolizing the prepared boron-binary oxidizer powders into the focal point of a CO₂ laser to initiate the particles. The emissions of the ignited particles were followed by filtered photomultiplier tubes (PMT) to obtain burn times. The particle ignition and consumption during combustion is followed as the peaking and decay of its emission pulse. The width of the pulse at 10% of its peak intensity is interpreted as the particle burn time.

The particles were fed into the laser beam by a custom-built screw feeder; its construction and operation were detailed in ²². The thread grooves of the screw accommodated powders to be tested. A mass of ~0.12 g of powder was loaded into 30 threads for every run. The screw is inserted into a cylindrical brass sleeve. A thin nozzle (metal tube) wedged into the thread groove is attached to the sleeve; when the screw rotates, it moves translationally inside the sleeve passing by the motionless nozzle. The particles loaded in the thread passing by the nozzle were blown out by air jet flown through the nozzle at 0.68 L/min. Across the nozzle, a receiving tube was inserted into the brass sleeve;

it fed the aerosol directly into the laser beam. The screw was slowly turned by a DC motor; the rate of rotation controlled the powder feed rate. The particles entrained into the air were channeled via a brass tube of internal diameter of 2.39 mm which extended up to 2 mm below the focal point of the laser beam. The infra-red beam generated by a Synrad Evolution 1215 sealed CO₂ laser was focused by a ZnS lens into a spot of ca. 260 μm diameter. The energy setting was maintained at 37.5W, much higher than the ignition threshold of powders tested, to ensure ignition of all particles crossing the beam. The complete experimental setup of the laser-initiated particle combustion is detailed in ²³.

The particle emission was captured by an optic fiber bundle trained at a region 2 cm above and 16 cm away from the opening of the brass feeder tube. The optical signals were fed into two Hamamatsu R3896-03 PMTs filtered at 700 and 800 nm. LabView software was used to process the signal acquired through a 16-bit PCI-6123 National Instruments board from the PMTs. An acquisition rate of 100,000 points per second in an 8 second window constituted a single run. Overlapping particle pulses were discarded. Several runs were collected and processed to collect at least 600 individual particle pulses. The width of the pulses interpreted as burn times were used to generate a burn time distribution using the kernel smoothing density function in MATLAB.

3.1.7 Aerosolized Particles Collection and Sizing

Particles passing through the feeder could be size classified compared to as prepared particles. Thus, for correlating particle sizes with their burn times, the particle size distributions were determined for the powders that have passed through the feeder. An SEM stub with carbon tape was placed 2.5 cm above the powder exit nozzle, perpendicular to the aerosolized particle stream. The feeder was operated, and carrier gas was flown under

identical conditions employed in combustion experiments; however, the laser was turned off. Particles were collected over a 15-20 s. Collected particles were examined using SEM. The images were processed for particle sizes as detailed in ²⁴. The obtained particle sizes were used to generate a distribution using kernel smoothing density function.

3.2 Results and Discussion

3.2.1 Oxidizer Characterization

Using XRD, the crystalline species in the oxidizers were identified and the traces were refined to obtain mass fractions of the recognized phases in each sample. The XRD traces of the milled oxidizers are shown in Figure 3.3. The peaks observed were generally diminished and broadened after milling. The compositions recovered from refining the XRD patterns for milled oxidizers are presented in Figure 3.2. Milled Bi_2O_3 (without CuO) shows the presence of bismuth sub-carbonate, $\text{Bi}_2\text{O}_2\text{CO}_3$ and bismuth oxide hydroxide carbonate, $(\text{BiO})_4\text{CO}_3(\text{OH})_2$. Due to the lack of structural details of the hydrated species, its mass percentage was not quantified. However, it is evident that a significant fraction of Bi_2O_3 reacted to form almost 30 wt. % of $\text{Bi}_2\text{O}_2\text{CO}_3$. No such degradation/reaction was observed for the milled CuO.

All three $\text{Bi}_2\text{O}_3\cdot\text{CuO}$ milled binary oxidizers have copper oxide and the mixed oxide phase, Bi_2CuO_4 which is the only phase expected for the equilibrated $\text{Bi}_2\text{O}_3\text{-CuO}$ binary system ²⁵. The mass fraction of Bi_2CuO_4 in the binary oxidizers, scales with mass of Bi_2O_3 in the oxidizer. The $75\text{Bi}_2\text{O}_3\cdot 25\text{CuO}$ binary oxidizer contains some Bi_2O_3 as separate phase along with CuO, yielding less than expected mixed oxide. Two other binary oxidizers contain Bi_2O_3 only in the mixed oxide.

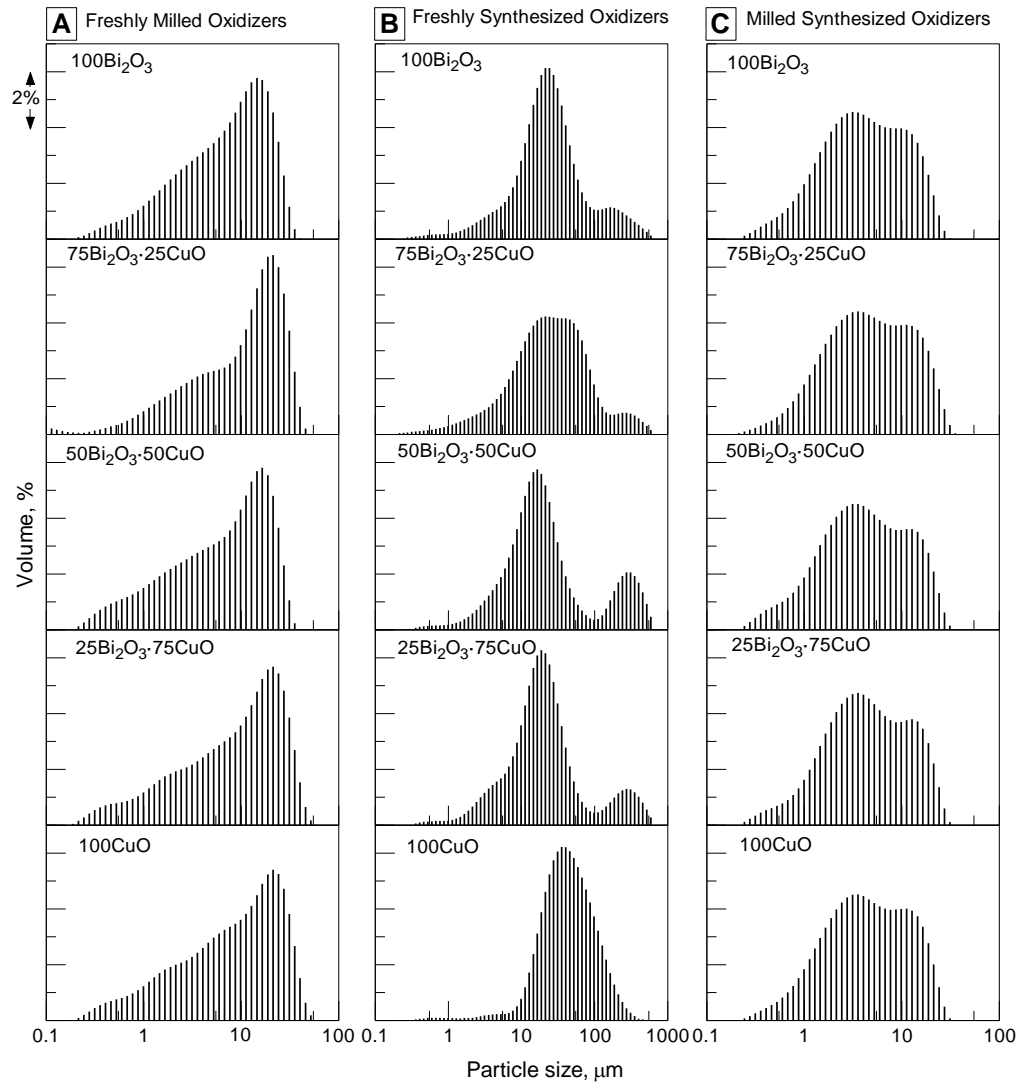


Figure 3.1 Particle size distribution of (A) freshly milled oxidizers (B) freshly synthesized oxidizers and (C) milled synthesized oxidizers.

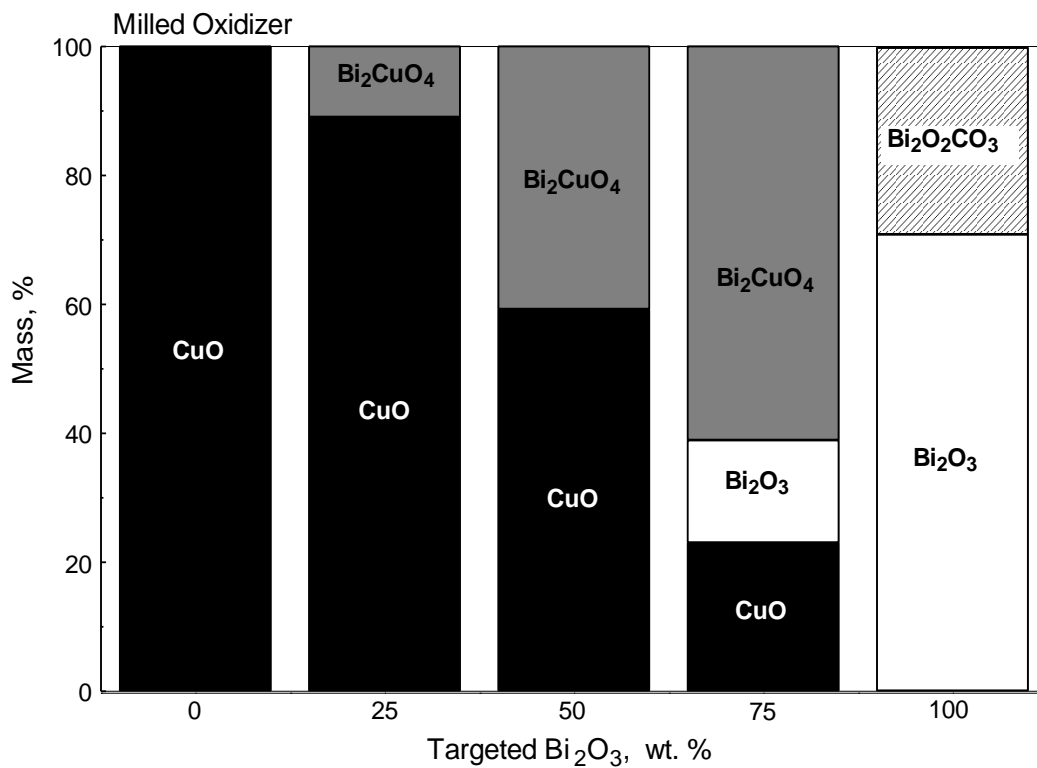


Figure 3.2 Compositional analysis of $\text{Bi}_2\text{O}_3 \cdot \text{CuO}$ milled oxidizers.

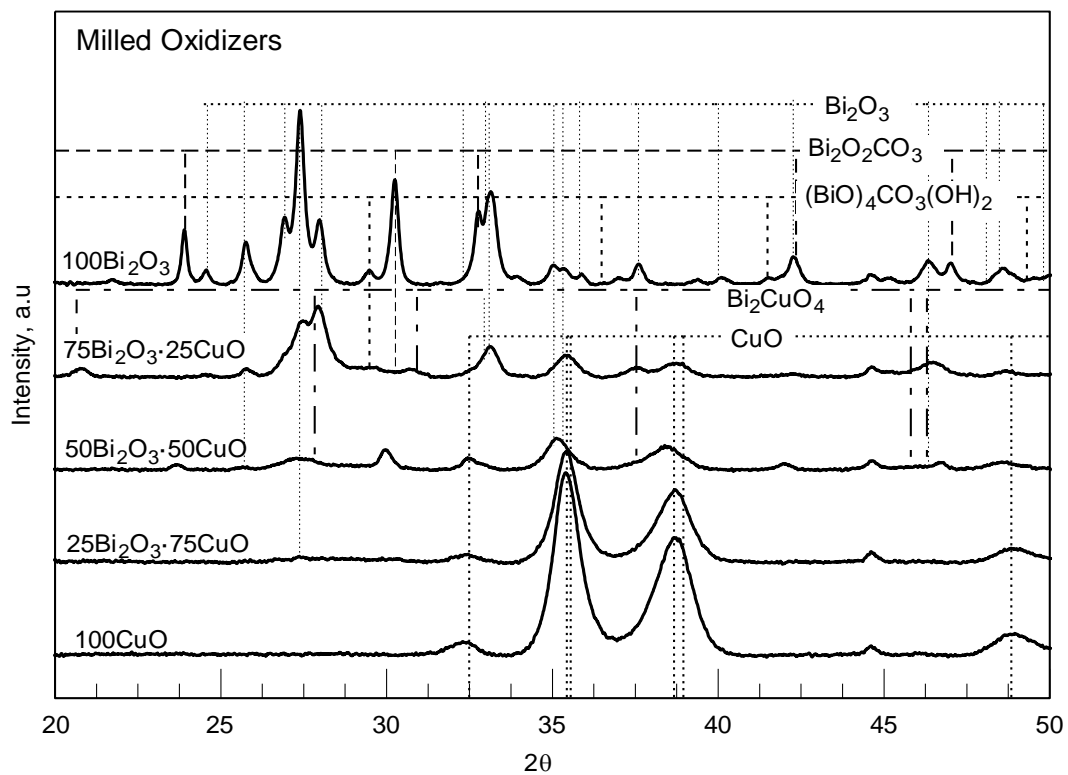


Figure 3.3 Background subtracted XRD traces of freshly prepared milled oxidizers.

A similar compositional plot for the synthesized $\text{Bi}_2\text{O}_3\cdot\text{CuO}$ oxidizers (analyzed before they were milled to reduce particle sizes) is presented in Figure 3.4. The respective XRD traces can be found in the Figure 3.5. The synthesized oxidizers showed sharp peak and were well crystalized. Also, the individual oxides Bi_2O_3 and CuO were uncontaminated. The synthesized binary oxidizers yielded the mixed oxide, Bi_2CuO_4 , the mass percentage of which scales with the amount of Bi_2O_3 in the binary oxidizer. The Bi_2O_3 -rich, $75\text{Bi}_2\text{O}_3\cdot 25\text{CuO}$ binary oxidizer does contain some Bi_2O_3 outside the mixed oxide, though much less than in the milled oxidizer of same target composition.

Based on the compositional detail of the freshly synthesized $\text{Bi}_2\text{O}_3\cdot\text{CuO}$ oxidizers, the boron-synthesized-oxidizers were prepared by adjusting the mass of oxidizer while fixing the boron mass at 2.5g to achieve an equivalence ratio of 21.6. The Table 4 provides the composition of the boron-synthesized-oxidizers powders.

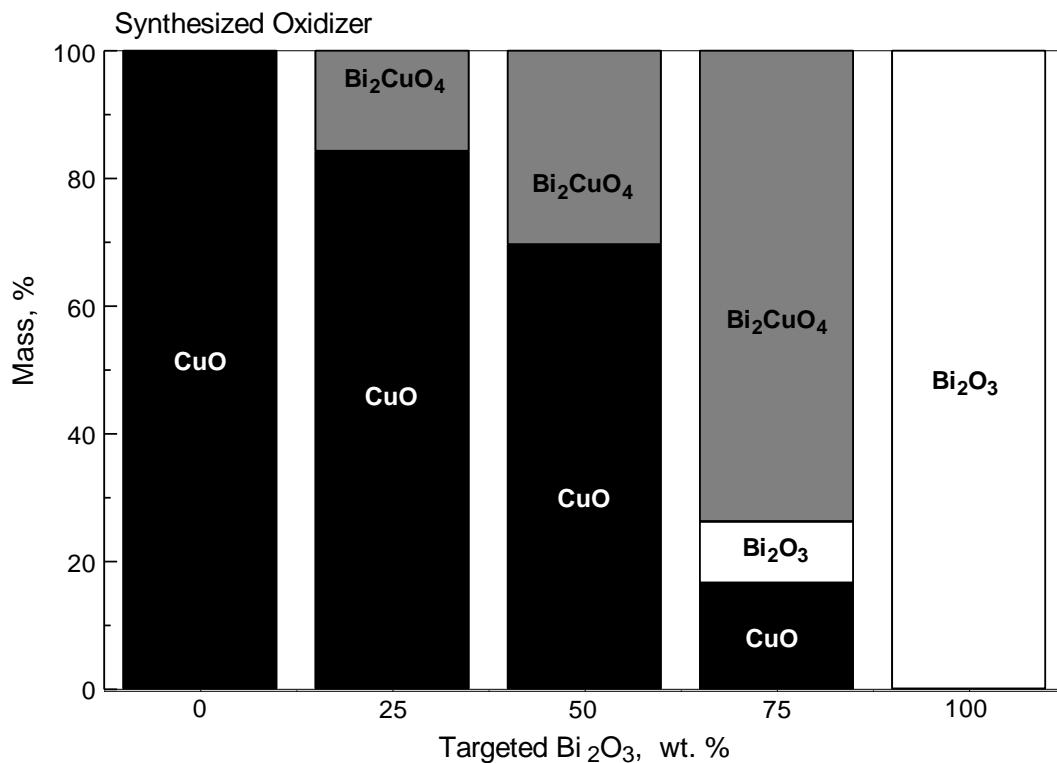


Figure 3.4 Compositional analysis of $\text{Bi}_2\text{O}_3 \cdot \text{CuO}$ synthesized oxidizers.

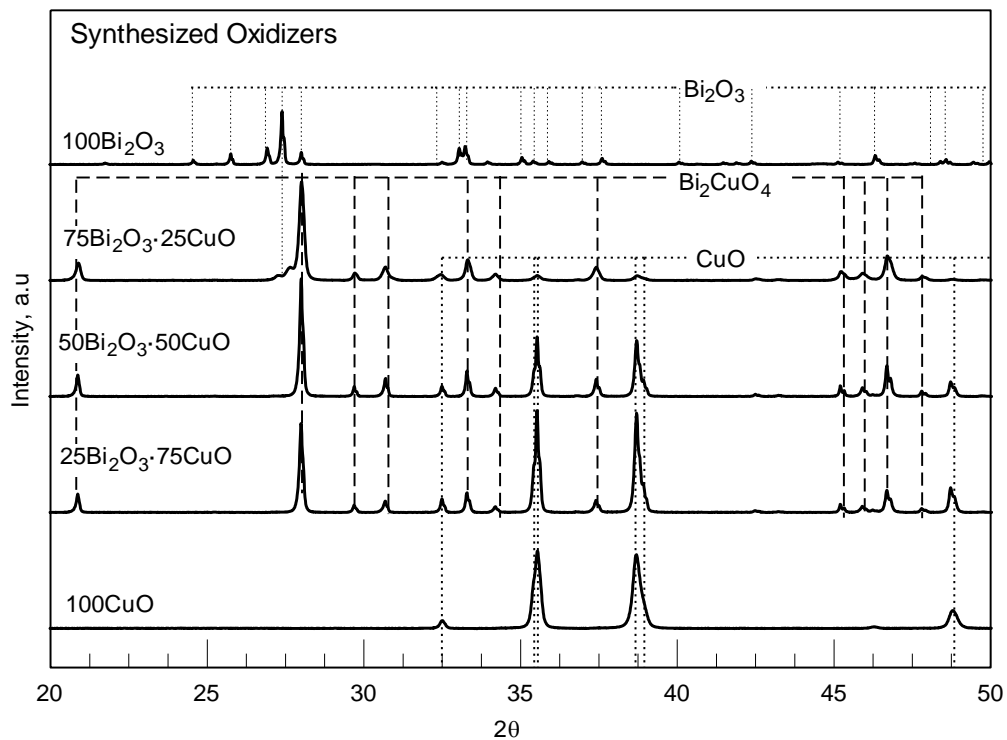


Figure 3.5 Background subtracted XRD traces of freshly prepared synthesized oxidizers.

Table 3.4 Prepared Compositions per Vial of Boron-Synthesized-Oxidizer Samples

Composition	Mass, g		Mass, %			Equivalence ratio
	Boron	Annealed Oxidizer	Boron	Bi ₂ O ₃	CuO	
B·100CuO (reference)	2.5	1.28	66.1	0	33.9	21.6
B·25Bi ₂ O ₃ ·75CuO		1.46	63.2	5.2	31.6	
B·50Bi ₂ O ₃ ·50CuO		1.69	59.6	10.4	30	
B·75Bi ₂ O ₃ ·25CuO		1.84	55.3	30.9	11.6	
B·100Bi ₂ O ₃ (reference)		2.5	50	50	0	

The compositional detail of the size reduced Bi₂O₃·CuO synthesized oxidizers is presented in Figure 3.6, the corresponding XRD traces may be found in Figure 3.7. The milling does not introduce significant iron contamination or degrade oxidizer as seen in the commercial milled Bi₂O₃. However, the mass percentage of the mixed oxide in the binary oxidizer compositions is seen to have increased while the remaining CuO is markedly diminished.

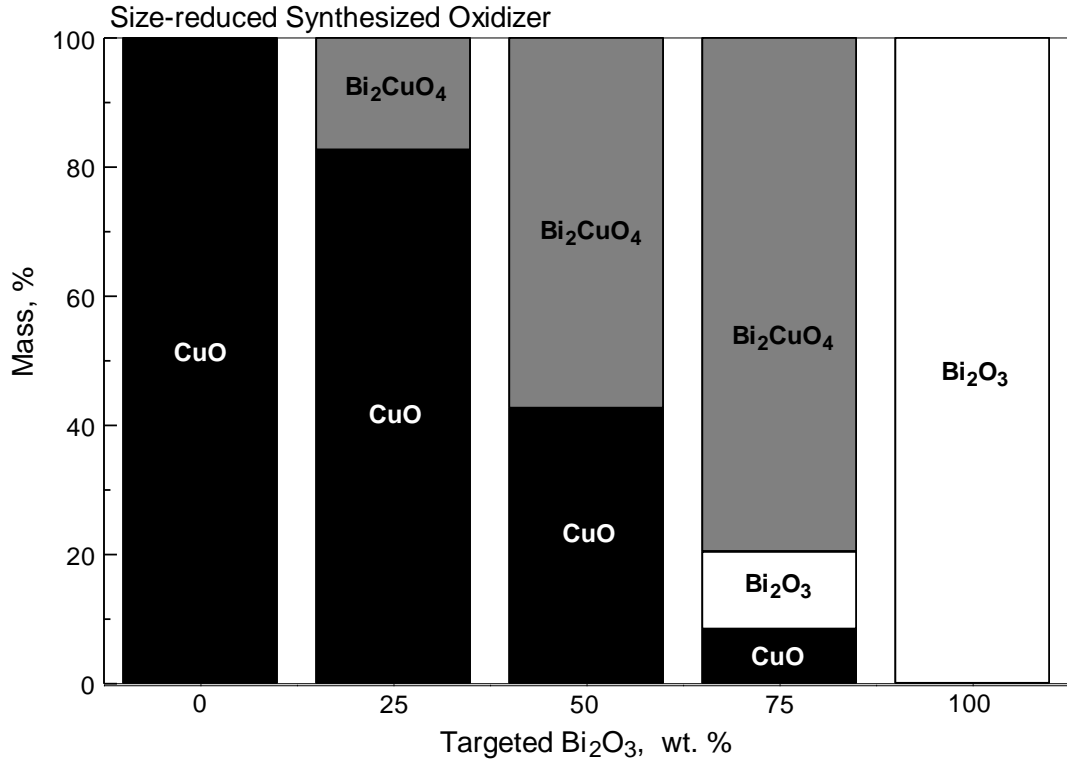


Figure 3.6 Compositional analysis of size reduced $\text{Bi}_2\text{O}_3 \cdot \text{CuO}$ synthesized oxidizers.

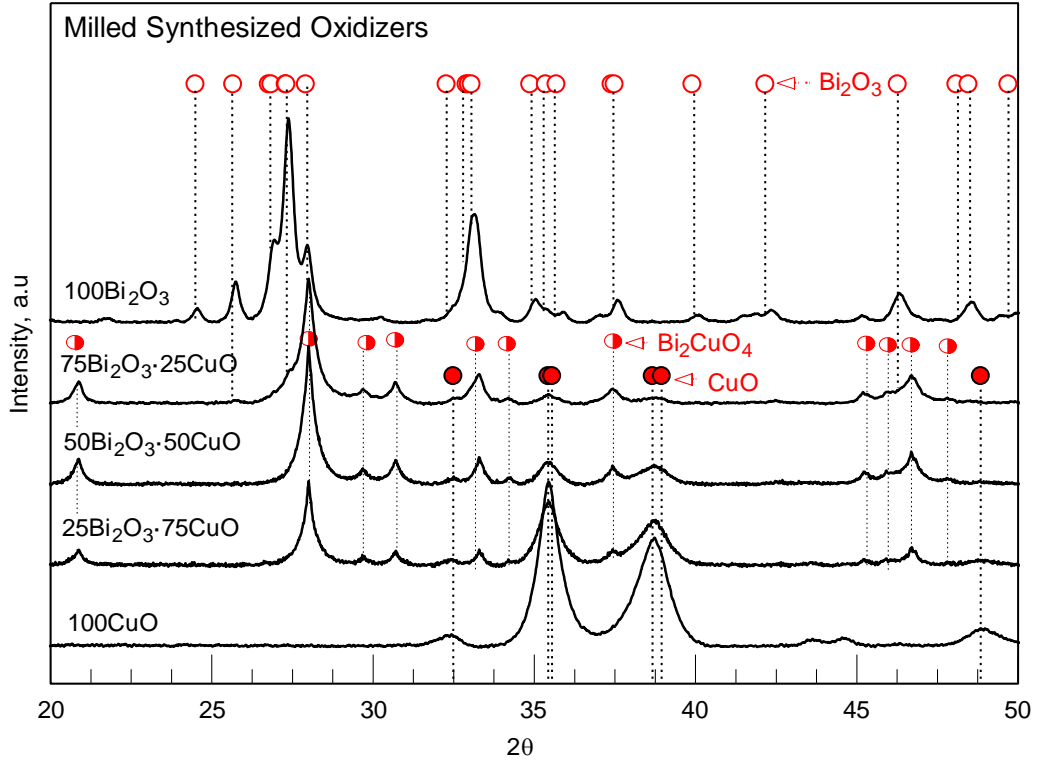


Figure 3.7 Background subtracted XRD traces of milled synthesized oxidizers.

The estimated mass percentages of Bi_2O_3 in all prepared oxidizers (from both separate Bi_2O_3 phase and from Bi_2CuO_4), across the different targeted compositions are shown in Figure 3.8. The synthesized oxidizers exhibit less than expected mass percentages of Bi_2O_3 (seen as black solid line) in the Bi_2O_3 -lean compositions. With increase in the target Bi_2O_3 in the oxidizer composition, its actual mass fraction approaches that expected. The estimated mass fraction of Bi_2O_3 and CuO phases in the synthesized oxidizers were used to calculate required boron mass to prepare reactive B-synthesized oxidizer composites to attain the equivalence ratio of 21.5. The milled oxidizers consistently had less than expected mass percentage of Bi_2O_3 across different compositions, possibly due combination of reasons such as degradation of oxides during milling and bias in estimation due to reduced crystallinity of certain phases.

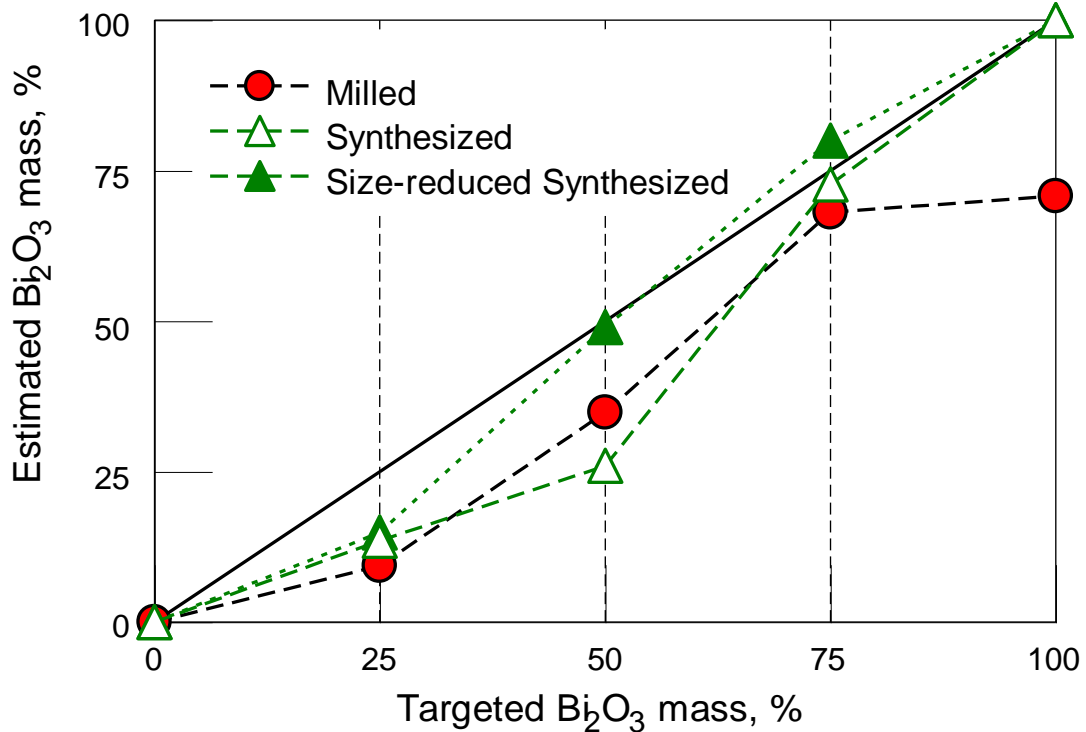


Figure 3.8 Estimated Bi_2O_3 mass percentage in the prepared Bi_2O_3 - CuO binary oxidizers.

3.2.2 Boron-Oxidizer Powder Morphology

SEM images of representative particles of the prepared B·synthesized oxidizer samples are presented in Figure 3.9. The images Fig. 3.9 (A) through (E) show the samples with increasing Bi_2O_3 mass percentage. The brightest particles correspond to the oxidizer consisting of metal oxides, the grey particles represent boron, while the darkest phase in the image is the carbon tape. The oxidizer is embedded in agglomerated boron particles as mostly submicron inclusions rather uniformly in all composites. The EDX shows a uniform dispersion of Bi_2O_3 and CuO phases in samples with binary oxidizers. A magnified surface of B·50 Bi_2O_3 ·50 CuO is shown in Figure 3.9 (F). The surface shows the smearing of the oxidizer, seen as a brighter phase, on the darker boron particle. Such smeared oxidizer was observed frequently in all the B·synthesized oxidizer samples.

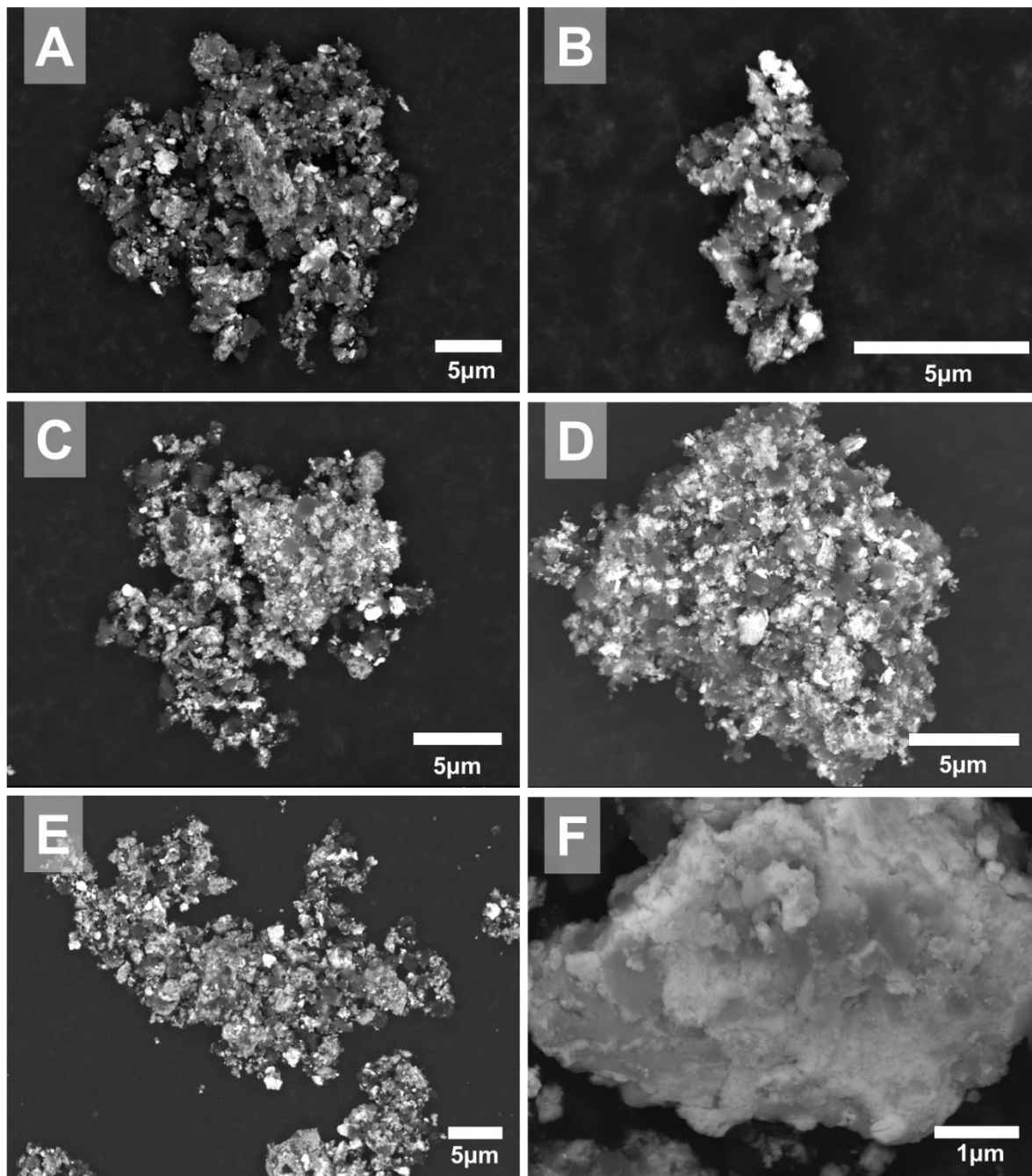


Figure 3.9 The SEM images of B-synthesized-oxidizers representative particles: (A) B·100CuO, (B) B·25Bi₂O₃·75CuO, (C) B·50Bi₂O₃·50CuO, (D) B·75Bi₂O₃·25CuO and (E) B·100Bi₂O₃ along with (F) magnified surface morphology of B·50Bi₂O₃·50CuO particle.

The representative particles of the prepared B-milled oxidizer samples are shown in Figure 3.10. These particles appear less well mixed compared to B-synthesized-oxidizer samples (Figure 3.9). Two distinct morphologies for distribution of oxidizer in the sample

were observed. In one case, boron served as a matrix with oxide inclusions as seen in Figure 3.10 (A-E). Alternatively, oxidizer served as the matrix with boron inclusions as seen in Figure 3.10 (F) for selected composite particles. Such “inverted” particles were observed in all the B-milled oxidizer samples.

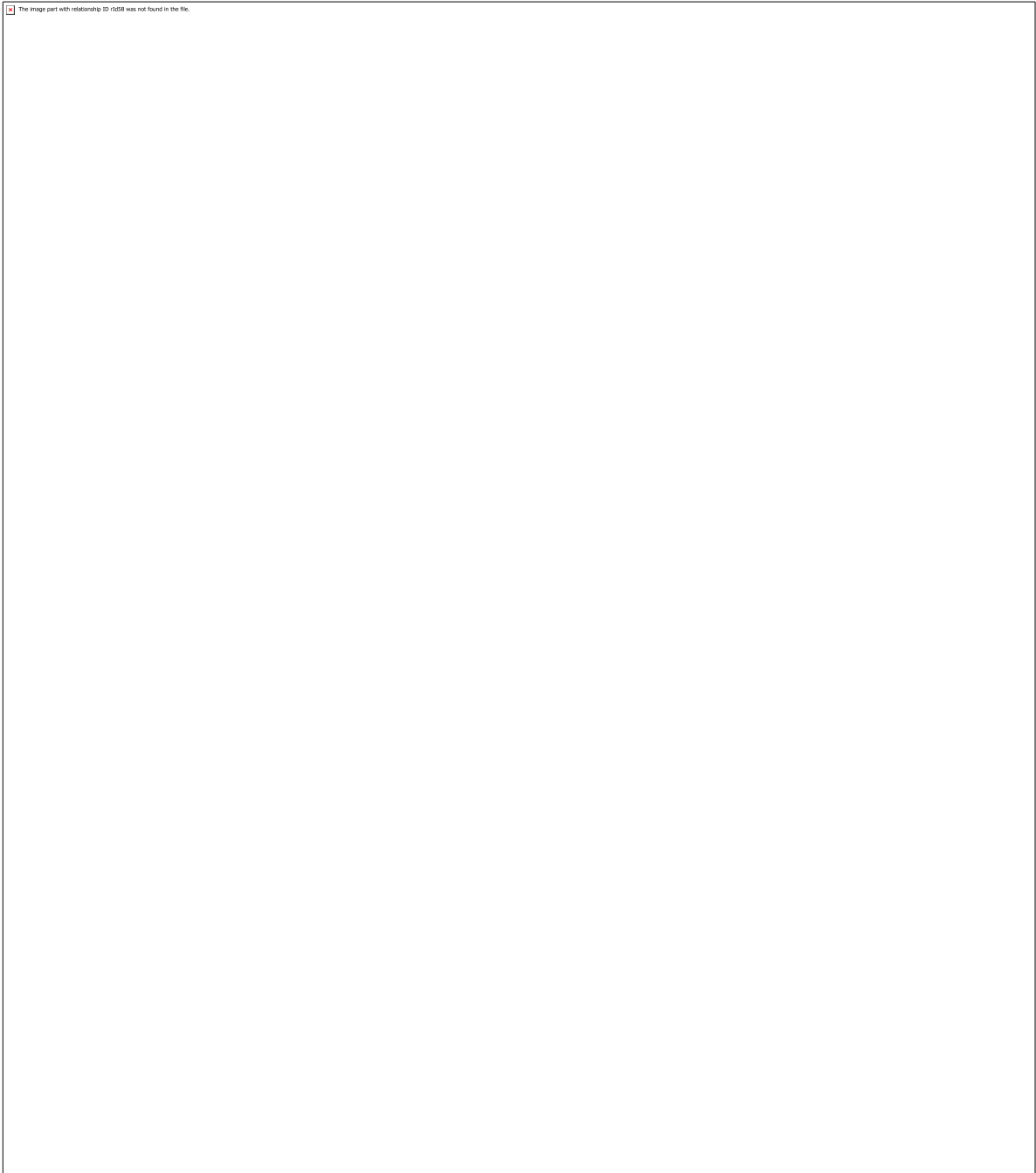


Figure 3.10 The SEM images of B-milled-oxidizers representative particles: (A) B·100CuO, (B) B·25Bi₂O₃·75CuO, (C) B·50Bi₂O₃·50CuO, (D) B·75Bi₂O₃·25CuO and (E) B·100Bi₂O₃ along with (F) surface morphology of large B·75Bi₂O₃·25CuO particle.

The particle size distributions of the prepared B-synthesized oxidizers and B-milled oxidizers samples are presented in Figure 3.11. All samples have similar bimodal distributions with peaks in the range 0.9-1.2 μm and 10-20 μm , with a significant volume fraction of fine particles.

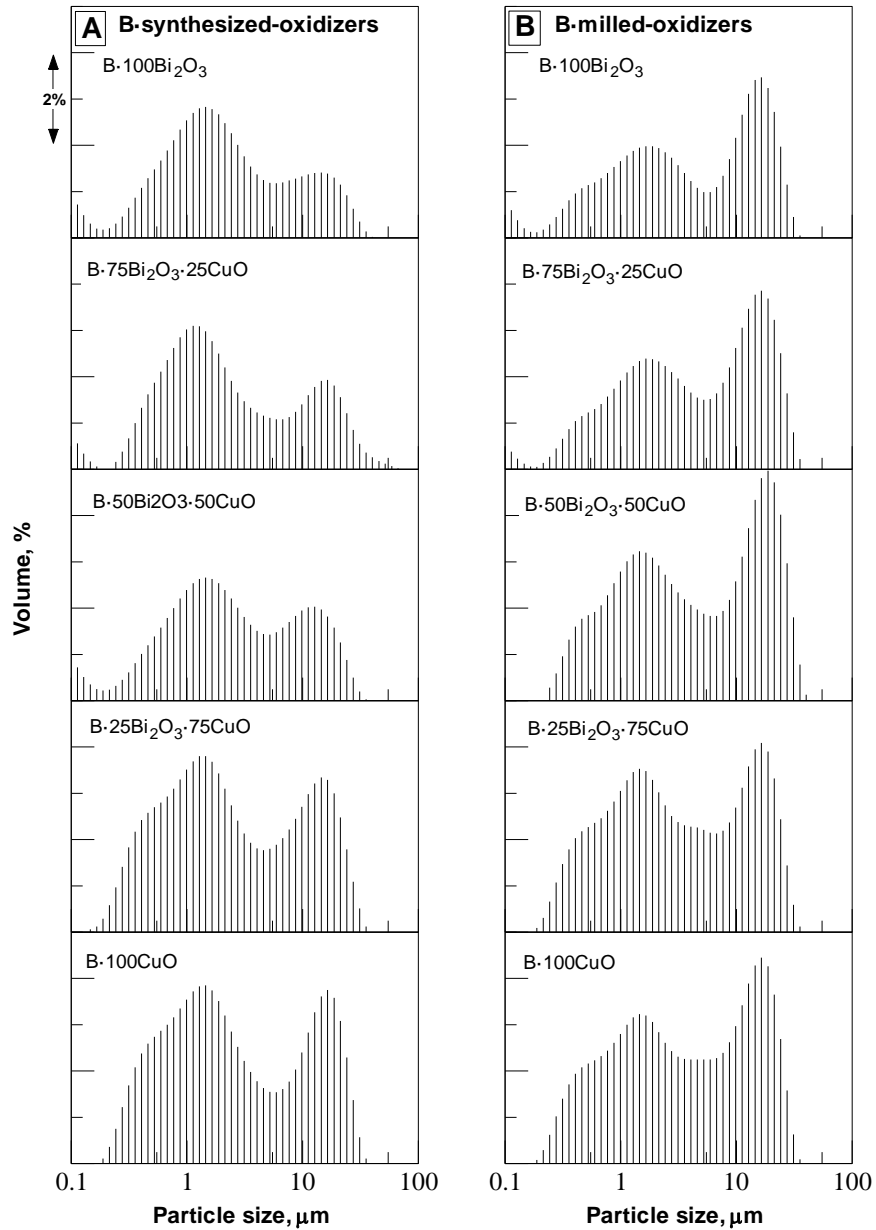


Figure 3.11 Particle size distribution of freshly prepared (A) B-synthesized-oxidizer and (B) B-milled-oxidizer samples.

3.2.3 Thermal Analysis

The TG and corresponding DTA traces of the oxidative runs of B-synthesized oxidizer composites heated at 5 K/min are presented in Figure 3.12. The prepared reactive composites show strong oxidative weight gain in the form of a step with an averaged inflection point of 490 °C. The corresponding DTA signals of the composites show a strong exothermic peak. The peak positions of the exotherms are comparable to one another. The composites exhibit different total mass gain at the end of the run at 700 °C. The reference B-100Bi₂O₃ composite oxidizes to the lowest final mass while the B-25Bi₂O₃-75CuO sample shows the highest mass gain of 66.7 % among all the B-synthesized oxidizer samples. Table 3.5 shows the theoretical mass gain of B-synthesized oxidizer powders along with the degree of oxidation achieved. The degree of oxidation is calculated as the percentage of the theoretical mass gain observed in the oxidative thermal analysis run within the experimental temperature range. It is evident that the B-25Bi₂O₃-75CuO sample achieves the highest degree of oxidation, achieving by 700 °C nearly 50 % of the theoretical maximum mass gain expected.

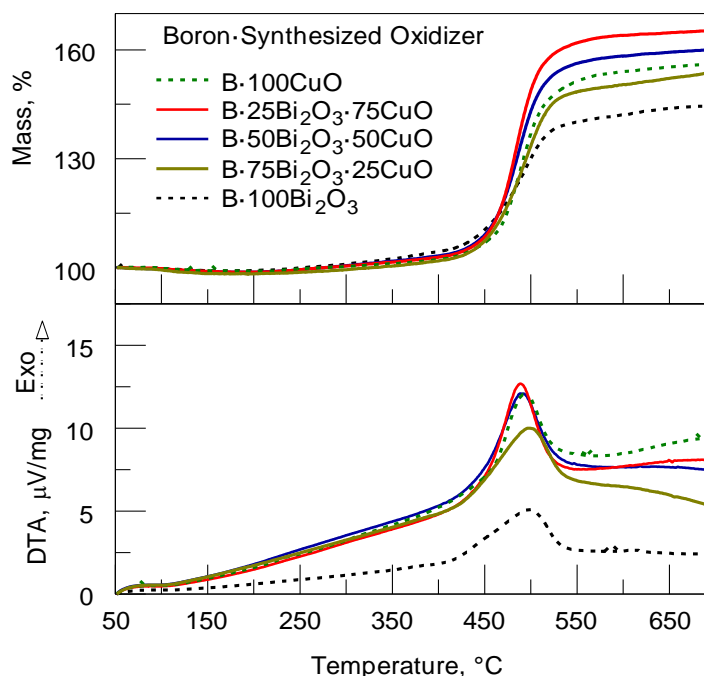


Figure 3.12 TG and corresponding DTA plots of B-synthesized oxidizer reactive composites heated at 5K/min in oxidative environment.

Table 3.5 Theoretical and Experimentally Observed Mass Gains and Degree of Oxidation Achieved by B-Synthesized Oxidizers

B-synthesized Oxidizer	Theoretical mass gain, %	Experimental mass gain, %	Degree of oxidation, %
B-100CuO (reference)	146.8	57.3	40.9
B-25Bi ₂ O ₃ -75CuO	140.2	66.7	49.9
B-50Bi ₂ O ₃ -50CuO	132.3	61.4	48.8
B-75Bi ₂ O ₃ -25CuO	127.6	55.5	44.8
B-100Bi ₂ O ₃ (reference)	110.9	45.5	42.0

The TG and corresponding DTA traces of prepared B-milled oxidizer composites in oxidative environment are similarly plotted in Figure 3.13. There is a minor mass loss by 100 °C and a singular mass gain similar to the B-synthesized oxidizer composites. The mass gain observable as a step is seen at a slightly higher temperature, with an averaged inflection point of 500 °C. The final mass gains of the B-milled oxidizer composites are

lower than for B-synthesized-oxidizer composites. The B-25Bi₂O₃-75CuO sample shows the highest mass gain of 55%. The corresponding DTA traces exhibit exotherms correlating to the mass gain steps; the exotherms appear to be sharper and stronger than for the B-milled oxidizer samples. Table 3.6 shows the theoretical mass gain, experimental mass gain and the degree of oxidation achieved by the B-milled powders similar to Table 3.5. A qualitatively similar trend is observed with the B-25Bi₂O₃-75CuO sample exhibiting the highest degree of oxidation among the other B-milled oxidizer powders. However, for a given composition, the B-milled oxidizer samples have a lower degree of oxidation as compared to B-synthesized oxidizers powders. Difference between the milled and synthesized oxidizer samples at the highest degree of oxidation values observed in the case of 25Bi₂O₃-75CuO composition is as much as 10 %.

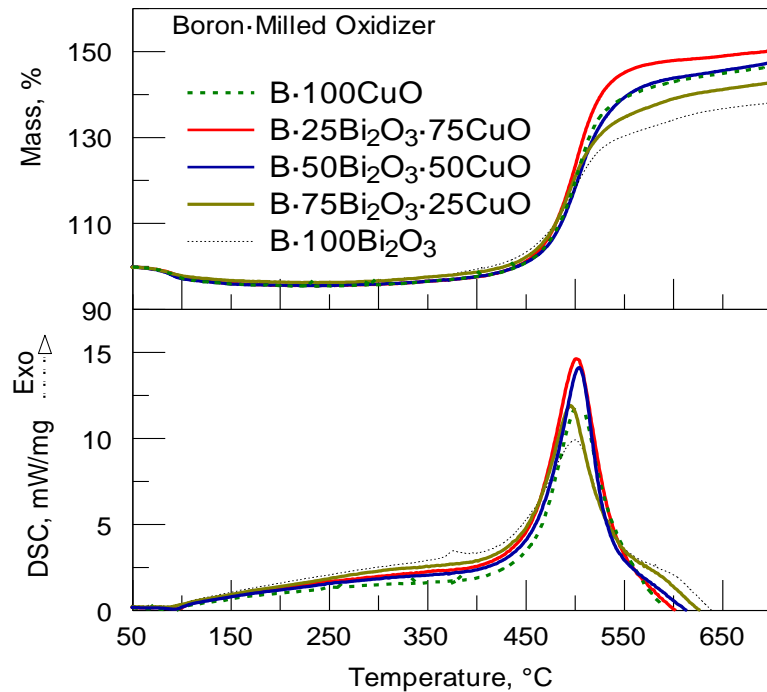


Figure 3.13 TG and corresponding DSC plots of B-milled oxidizer reactive composites heated at 5 K/min in oxidative environment.

Table 3.6 Theoretical and Experimentally Observed Mass Gains and Degree of Oxidation Achieved by B-Milled Oxidizers

B-milled Oxidizer	Theoretical mass gain, %	Experimental mass gain, %	Degree of oxidation, %
B·100CuO (reference)	146.809	51.83	35.31
B·25Bi ₂ O ₃ ·75CuO	140.212	54.59	38.93
B·50Bi ₂ O ₃ ·50CuO	132.35	51.02	38.54
B·75Bi ₂ O ₃ ·25CuO	122.808	46.53	37.88
B·100Bi ₂ O ₃ (reference)	110.998	41.75	37.61

The DTG plots of the TG traces of both B-synthesized-oxidizer and B-milled-oxidizer reactive composites heated in air, seen in Figures 3.12 and 3.13 respectively, are presented in Figure 3.14. In both sets of prepared samples, the B·25Bi₂O₃·75CuO samples exhibit the strongest peak values as previously noted in their corresponding DTA/DSC plots. The DTG traces are further plotted in logarithmic scale to resolve the low temperature features seen in the insets. In the case of B-synthesized oxidizer samples, the DTG value increases in strength as the mass percentage of Bi₂O₃ in the sample increases. With the B·CuO and B·Bi₂O₃ samples, exhibiting the lowest and the highest DTG values in the temperature range 200-400°C. A qualitatively similar behavior is observed for B-milled oxidizer samples. However, the differences between the samples is not as strong as for B-synthesized oxidizer samples.

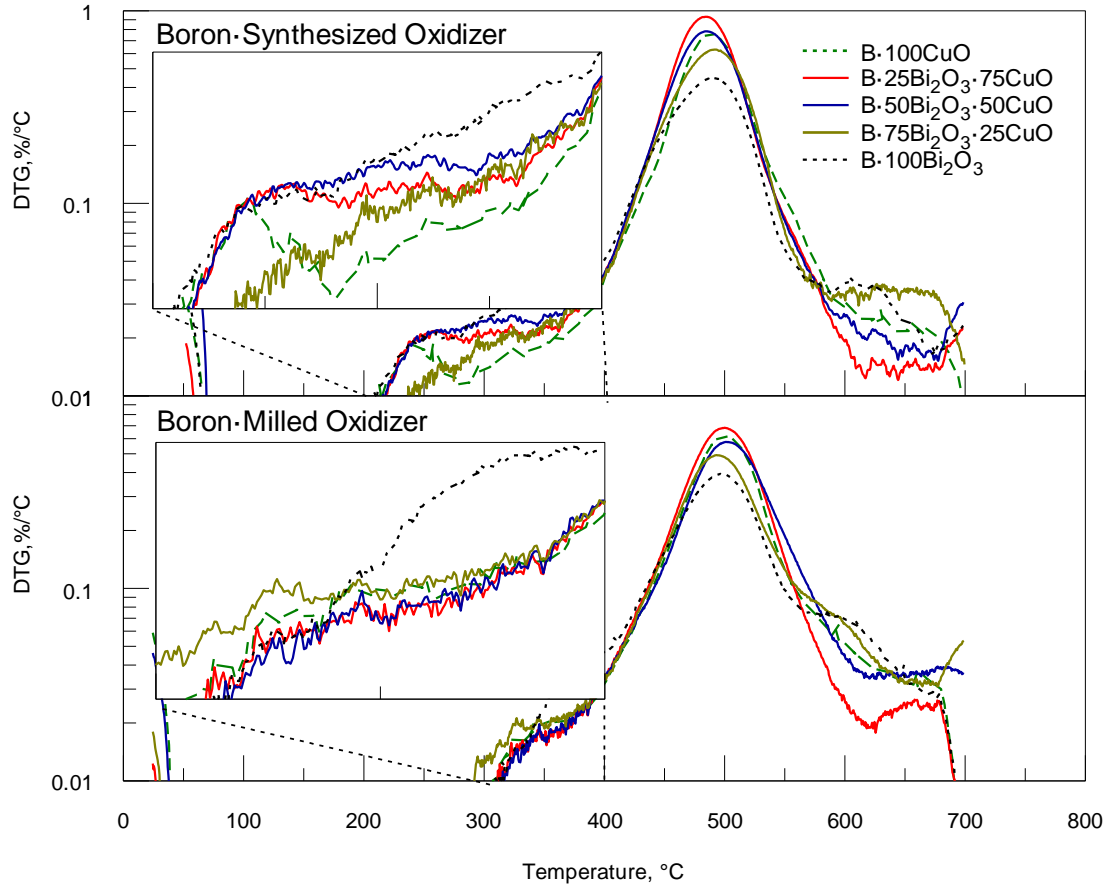


Figure 3.14 The DTG plots of B-synthesized oxidizer and B-milled oxidizer reactive composites heated at 5K/min in oxidative environment.

The inert environment runs with higher loaded sample mass heated at 40 K/min are discussed separately because they offer a better feature resolution. TG and corresponding DTA measurements for B-synthesized oxidizer are shown in Figure 3.15. The samples exhibit a minor mass loss of ~ 5 wt. % between approximately 100 and 350 °C. The DTA of the samples exhibit exotherms spanning 500 – 650 °C (somewhat above the temperature of the main oxidation step observed in presence of external oxidizer, Figure 3.12) without any corresponding mass change. The exotherm observed in B-100Bi₂O₃ comprised two overlapping peaks while the exotherm observed for B-100CuO is a single peak. The exotherms of samples containing Bi₂O₃ in their oxidizers, exhibit the bimodal feature seen in B-100Bi₂O₃ end member.

The TG and corresponding DTA of B·milled-oxidizer samples run in inert atmosphere are similarly plotted in Figure 3.16. The TG and DTA features of the B·milled-oxidizer samples are qualitatively comparable to the B·synthesized-oxidizer samples. A notable difference in behavior between the two sets of samples was observed in the peak shape of B·25Bi₂O₃·75CuO, which was a single peak similar to the reference sample B·100CuO.

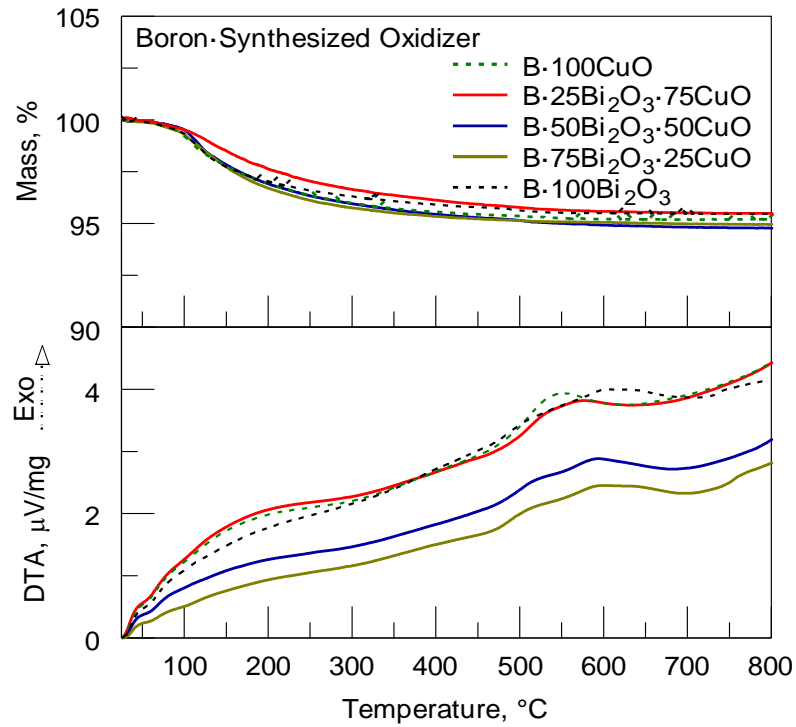


Figure 3.15 TG and corresponding DTA plots of B·synthesized oxidizer reactive composites heated at 40 K/min in inert environment.

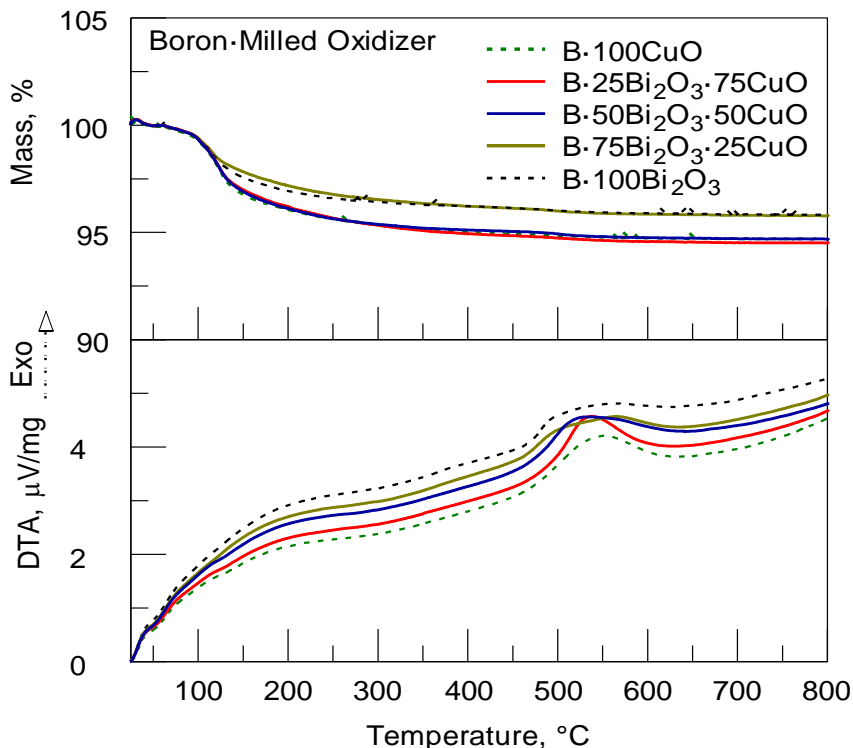


Figure 3.16 TG and corresponding DTA plots of B·milled oxidizer reactive composites heated at 40K/min in inert environment.

To capture the trends in both sets of reactive samples with synthesized and milled oxidizers, characteristic values recovered from thermo-analytical measurements are plotted as a function of Bi₂O₃ weight percentage in oxidizer in Figure 3.17. The degree of oxidation (in %) is shown in Figure 3.17 (A) following comparisons with the maximum possible mass gain in Tables 3.5 and 3.6. The highest rates of oxidation measured from the derivative of TG traces (DTG) are presented in Figure 3.17 (B). Similar plots presenting the area under the exotherms observed in both oxidative and inert environment runs are plotted in Figures 3.17 (C) and (D) respectively.

As seen in Figure 3.17 (A), for composites with both milled and synthesized oxidizers, the samples containing 25 wt. % Bi₂O₃, B·25Bi₂O₃·75CuO achieve the highest degree of oxidation amongst other compositions. The boron-synthesized oxidizer samples in general have higher oxidized composites as compared to B·milled oxidizers samples,

with a difference of 10 % between the samples containing oxidizer with 25 wt. % Bi_2O_3 . Similarly, the greatest rate of oxidation implied by the peak of DTG occurs for samples containing 25 wt. % Bi_2O_3 for both milled and synthesized oxidizers (Figure 3.17 (B)).

The same general trend for the reaction rates is implied by the exothermicity of peaks observed in both inert and oxidative thermal analysis runs (Figure 3.17 (C) and (D)): the maximum rates are observed for the samples containing oxidizers with 25 wt. % Bi_2O_3 . The reaction rates for CuO-rich compositions of B-milled oxidizer samples appear to be lower than the rates for the corresponding B-synthesized oxidizer samples (Figure 3.17 (D)).

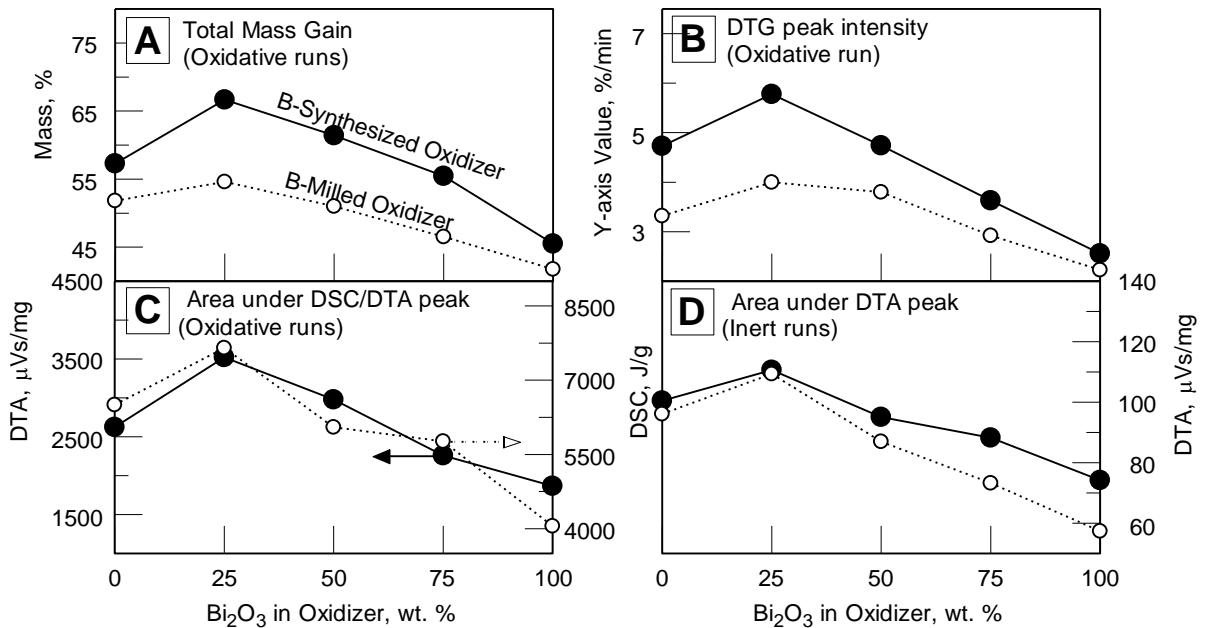


Figure 3.17 The measurements obtained from thermal analysis runs: (A) Total mass gain in oxidative runs, (B) DTG peak intensity in oxidative runs, (C) Area under DSC/DTA peaks in oxidative runs, and (D) Area under DTA peak in inert runs, plotted as a function of Bi_2O_3 in oxidizer.

3.2.4 Ignition Temperature

The ignition temperatures of the prepared B-synthesized oxidizer samples in air are presented as a function of heating rates in Figure 3.18. The end member B·100CuO exhibits the highest ignition temperature; conversely, the other end member, B·100Bi₂O₃ has the lowest ignition temperatures. For all materials, the ignition temperatures increase with the heating rate in a similar fashion. Despite relatively high error bars, the ignition temperatures appear to increase slightly with the amount of CuO.

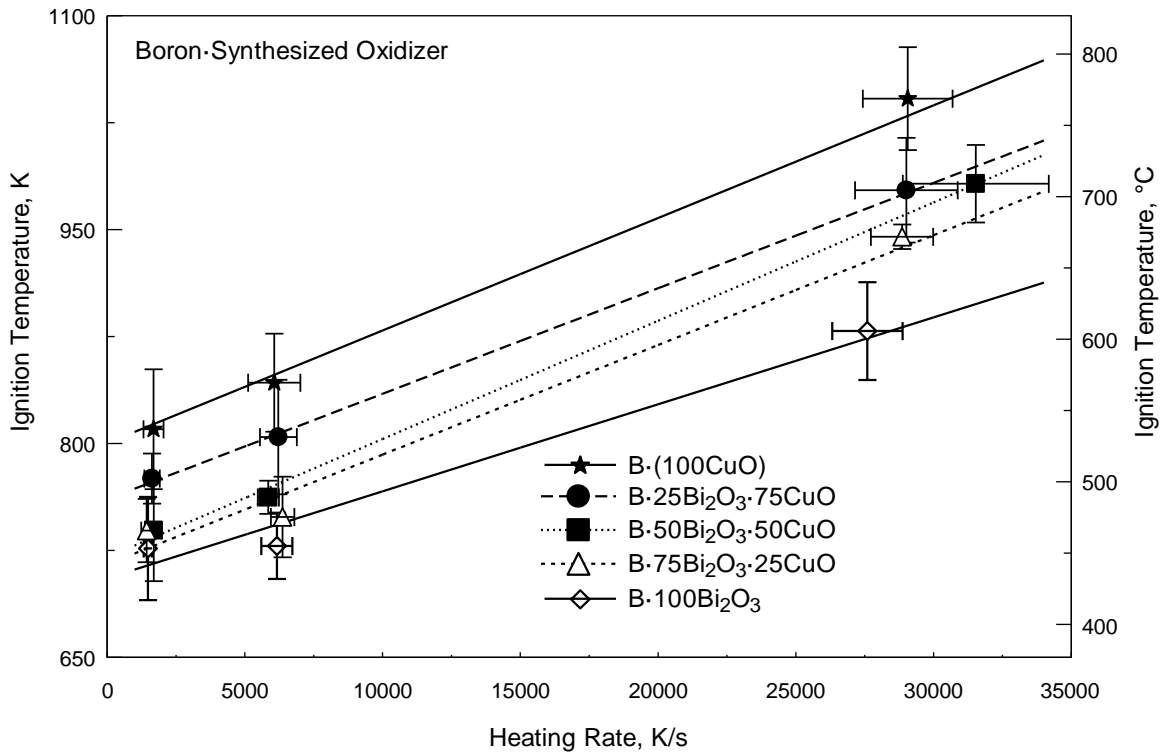


Figure 3.18 Ignition temperature of B-synthesized oxidizer samples in air as a function of heating rate.

A similar plot of ignition temperatures of the B-milled oxidizer samples as a function of heating rate is presented in Figure 3.19. The range of ignition temperatures is generally the same as in Figure 3.18. The end member B·100CuO still shows the highest ignition temperature. There is still a clear trend of the ignition temperature increasing with

the heating rate. However, differences in the specific ignition temperatures for other samples are hard to identify due to large measurement uncertainties.

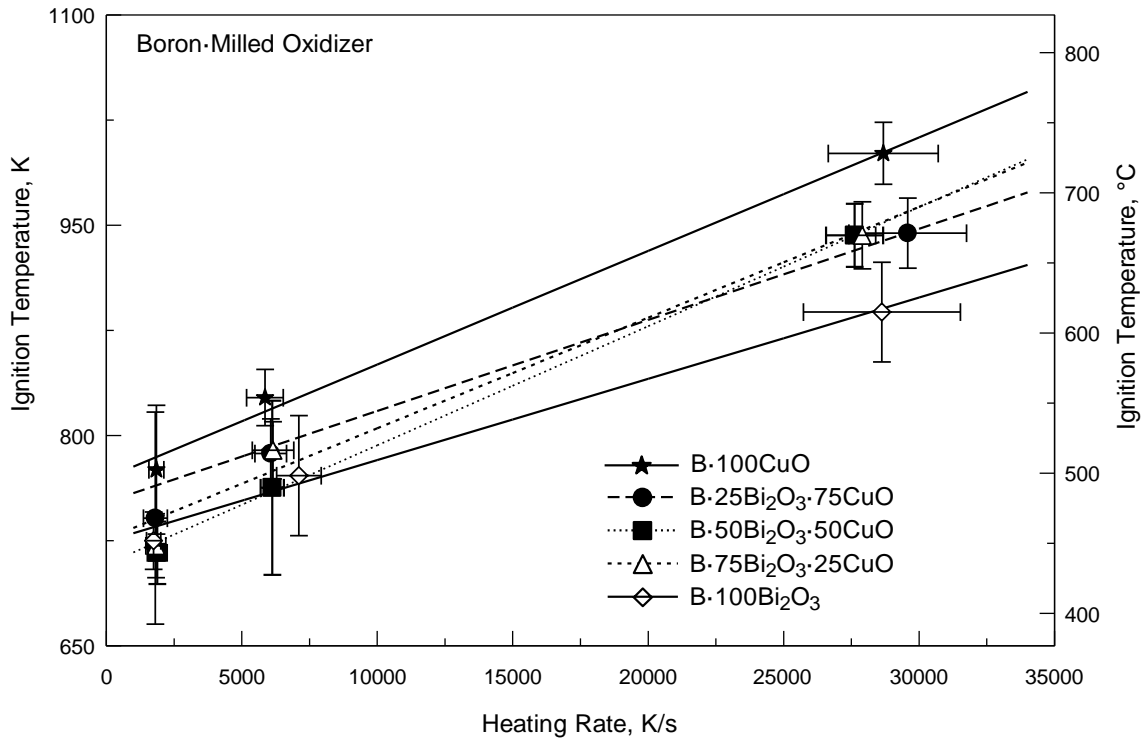


Figure 3.19 Ignition temperature of B-milled oxidizer samples in air as a function of heating rate.

3.2.5 Correlation of the Ignition Temperature with Reaction Observed in Thermos-Analytical Experiments

Figure 3.20 presents the ignition temperatures and the onset of mass gain observed in oxidative thermal analysis runs for the B-synthesized oxidizers, in a Kissinger plot. Black filled dots indicates the ignition measurements while the white un-filled dot represents TG onsets of mass gain. The black dotted lines represent the fit line of the wire ignition data while two red dotted lines represents the standard deviation. The difference between expected onsets for a perfect fit and onset temperatures obtained from thermal analysis is marked by the black arrow line plotted in Figure 3.20. All the compositions have onset

temperatures that line reasonably well with the wire ignition data. B·25Bi₂O₃·75CuO composition has onset temperature that is the closest to the expected value amongst all the other compositions. The low temperature oxidation possibly drives ignition at higher heating rates for all the prepared B·synthesized oxidizers. The oxidation of boron in the prepared fuel-rich compositions are due to both heterogenous oxidation between boron and added oxidizer and boron with surrounding ambient oxygen.

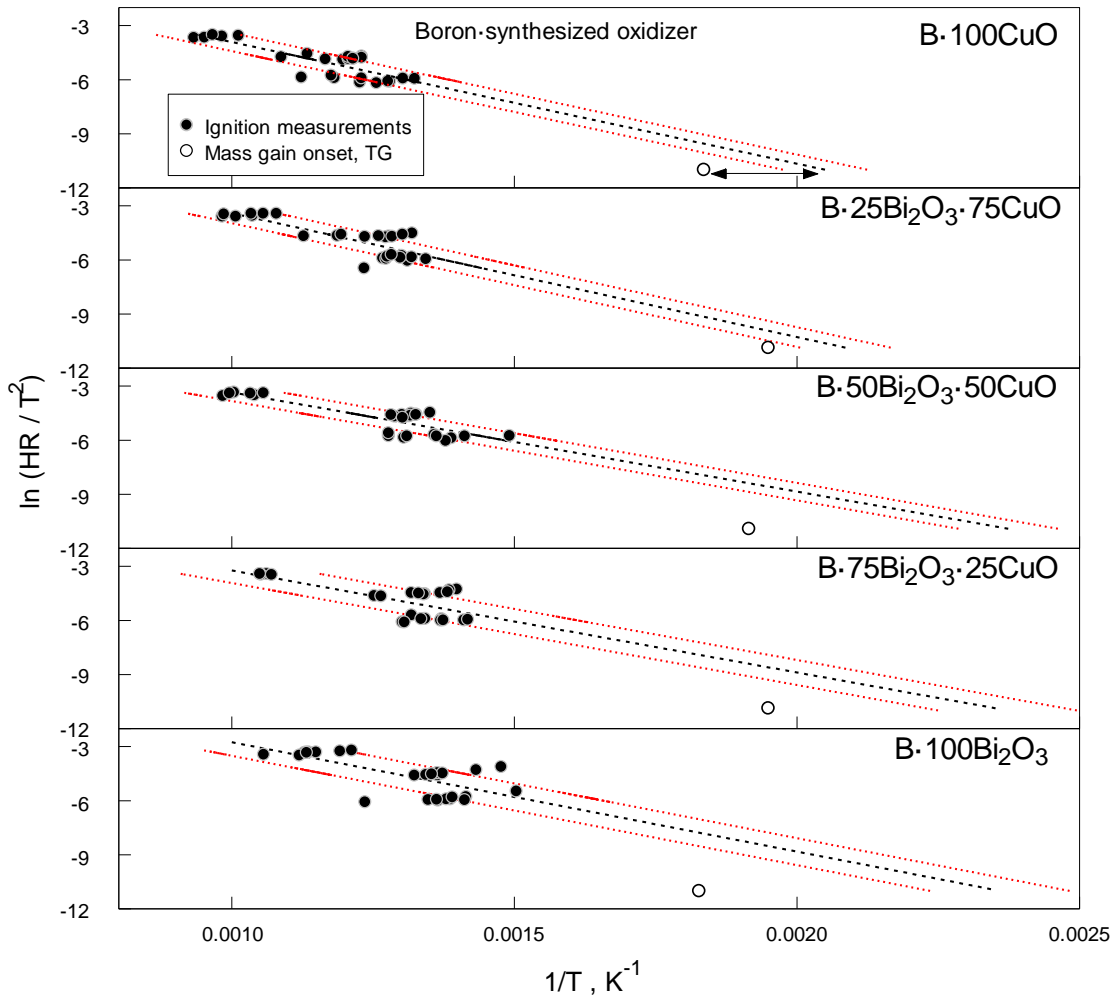


Figure 3.20 Kissinger plots correlating inverse ignition temperatures, $1/T$, with the inverse temperatures of the onset of mass gain observed in the oxidizing TG runs. The vertical scale is a variable determined by the heating rate, HR.

The differences between the experimental inverse temperatures of the mass gain onset in TG and the inverse temperatures based on the extrapolated kinetic trends using

ignition measurements are plotted in Figure 3.21 as a function of the oxidizer composition. The aligning of the experimental value with the expected one may be interpreted to suggest a stronger contribution of heterogeneous redox reactions as ignition drivers. In agreement with Figure 3.20, a smallest absolute discrepancy is noted for B·25Bi₂O₃·75CuO.

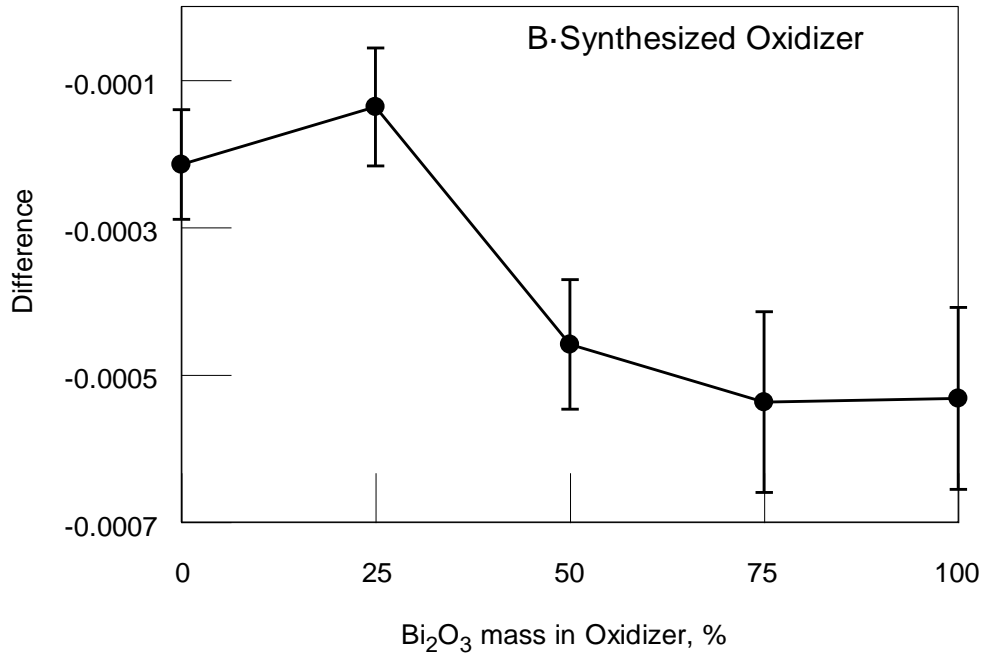


Figure 3.21 The difference between the experimentally obtained inverse temperature for onset of mass gain and inverse temperature projected by extrapolating the kinetic trend for ignition for B-synthesized oxidizer composites to low heating rates.

Similar data processing for B-milled oxidizer composites is shown in Figures 3.22 and 3.23, where Kissinger plots extrapolating the kinetic trends implied by ignition measurements to low heating rates are shown in Figure 3.22 and specific comparisons of the mass gain onset points observed in TG and those implied by the above extrapolation presented in Figure 3.23. For the B-milled oxidizer composites, mass gain onset occurs close temperatures for all samples. At the same time, the discrepancies between the actual and extrapolated mass gain onset points are somewhat greater than for B-synthesized oxidizer composites. The experimental mass gains occur at noticeably higher temperatures

than anticipated based on the kinetic trend observed for ignition experiments. The discrepancy is particularly high for B-50Bi₂O₃-50CuO composite. One interpretation of this observation can be that oxidation of boron and reduced Bi and Cu by ambient oxidizers plays an increasingly greater role in ignition of the B-milled oxidizer composites.

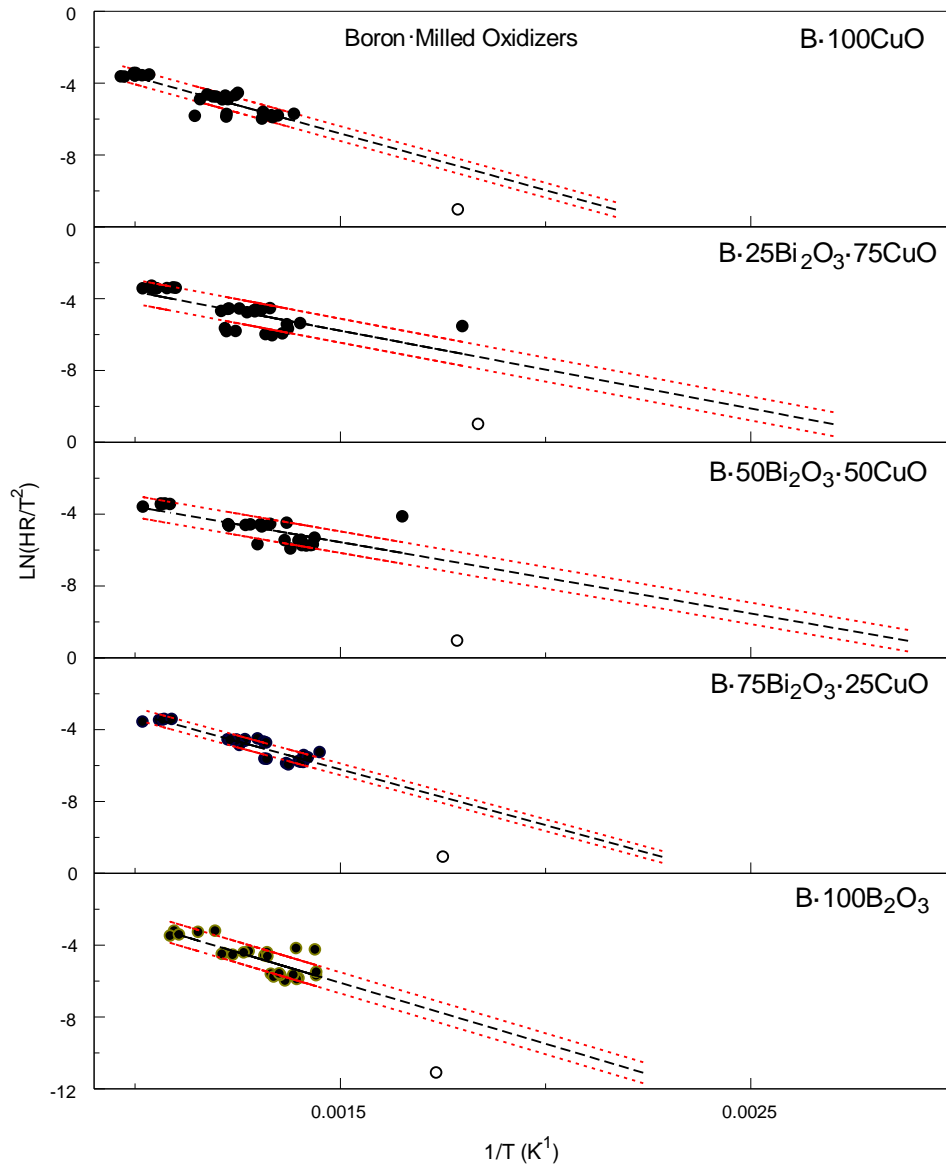


Figure 3.22 Kissinger plots correlating inverse ignition temperatures, $1/T$, with the inverse temperatures of the onset of mass gain observed in the oxidizing TG runs for B-milled oxidizer composites. The vertical scale is a variable determined by the heating rate, HR.

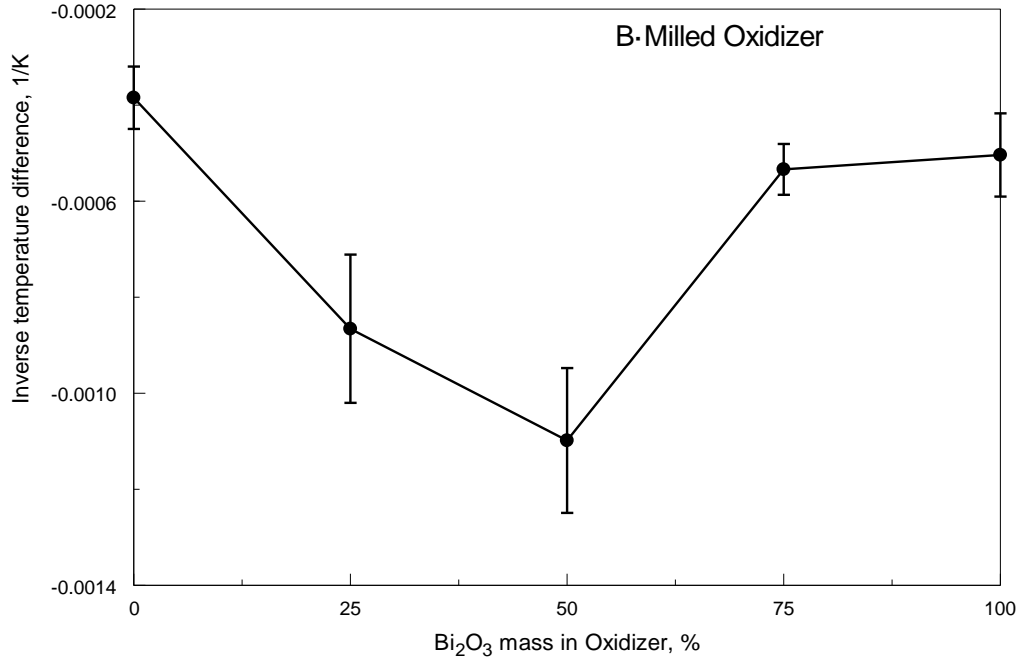


Figure 3.23 The difference between the experimentally obtained inverse temperature for onset of mass gain and inverse temperature projected by extrapolating the kinetic trend for ignition for B-milled oxidizer composites to low heating rates.

3.2.6 Particle Combustion in Air

Because both composites with milled and synthesized oxidizers exhibit qualitatively similar behaviors in the tests discussed above, only the samples with B-milled oxidizer were tested in particle combustion experiments. Representative emission pulses produced by burning particles ignited by the laser beam in air are presented in Figure 3.24. All pulses are qualitatively similar to one another with a single peak and oscillatory decay. Double-peak pulses typically associated with boron combustion were not observed.

The width of these pulses was interpreted as burn times of particles. The time distributions are presented in Figure 3.25. All samples except for B-100Bi₂O₃ exhibit normal distributions while a bimodal distribution is noted for B-100Bi₂O₃. The average burn times for different compositions do not differ significantly.

The particle size distribution of the B-milled oxidizer samples fed to and captured above the laser beam (with no CO₂ laser emission) are presented in Figure 3.26. The

distributions appear to consist of two overlapping peaks with the stronger peak between 1 and 2 μm .

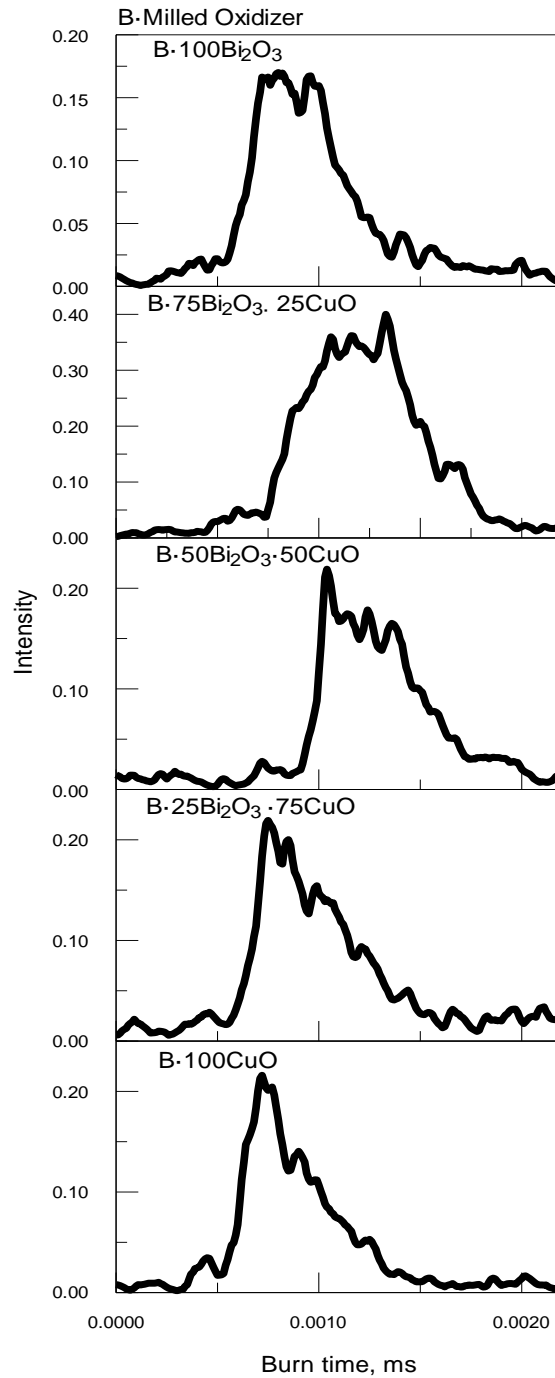


Figure 3.9 The representative emission pulses observed in laser-assisted particle combustion experiments in air for the prepared B-milled oxidizer samples.

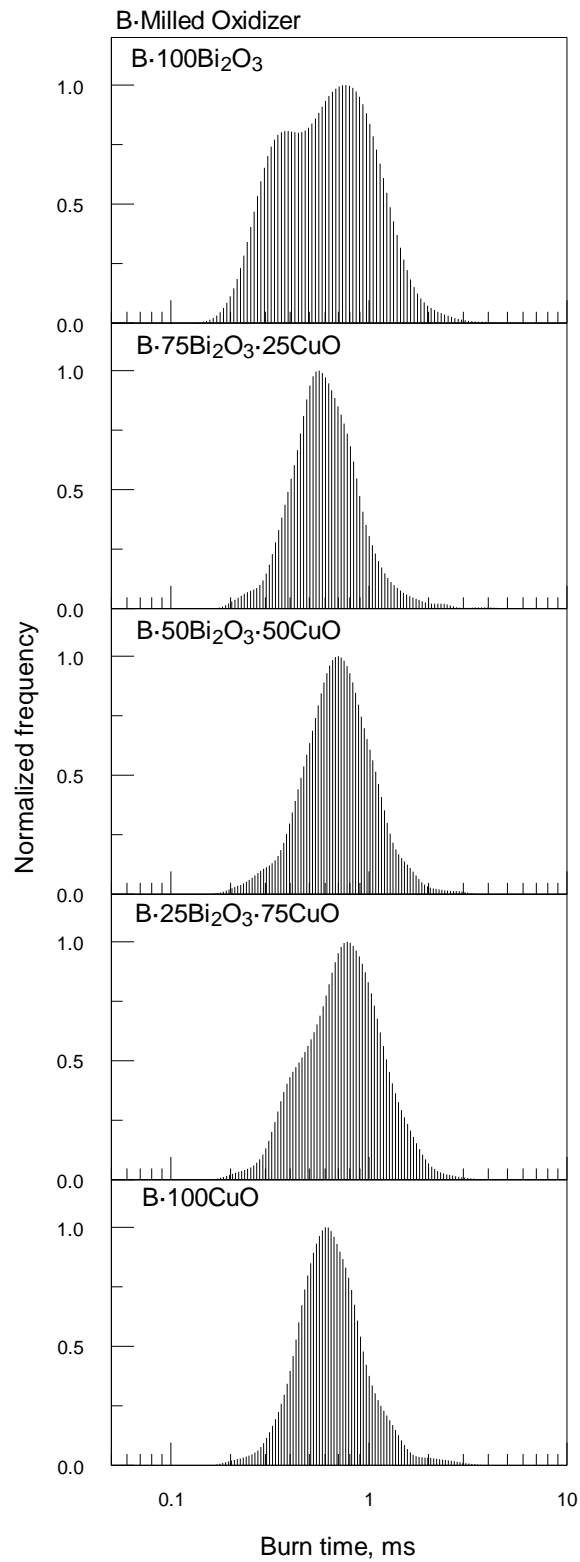


Figure 3.25 The burn time distributions of the prepared B-milled oxidizer samples obtained from particle combustion experiments in air.

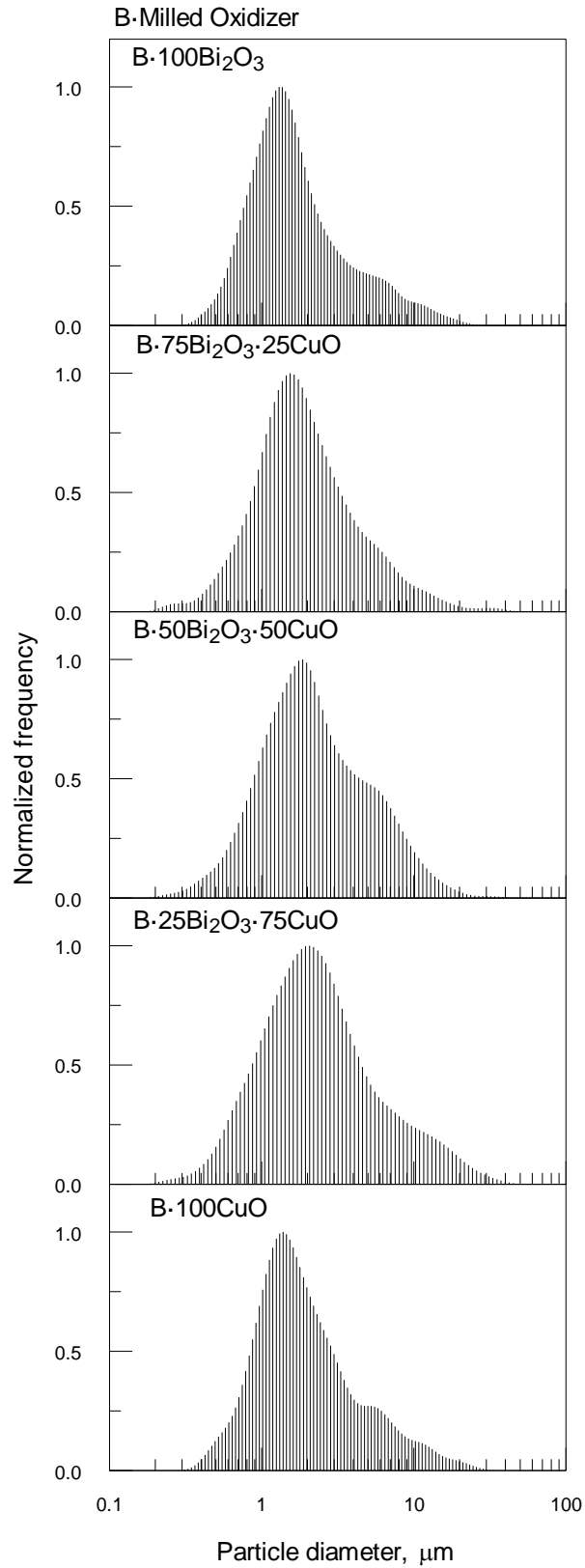


Figure 3.26 The aerosolized particle size distributions of the prepared B-milled oxidizer samples in the laser-assisted particle combustion experimental setup.

The burn time – particle size correlations for the B-milled oxidizer samples combusting in air are presented in Figure 3.27. No difference among correlations was observed for different compositions prepared. All samples exhibited a burn time approximately proportional to $d^{0.45}$, where d is particle size. The combustion times are noticeably shorter than those for similarly sized pure boron particles burning in air.

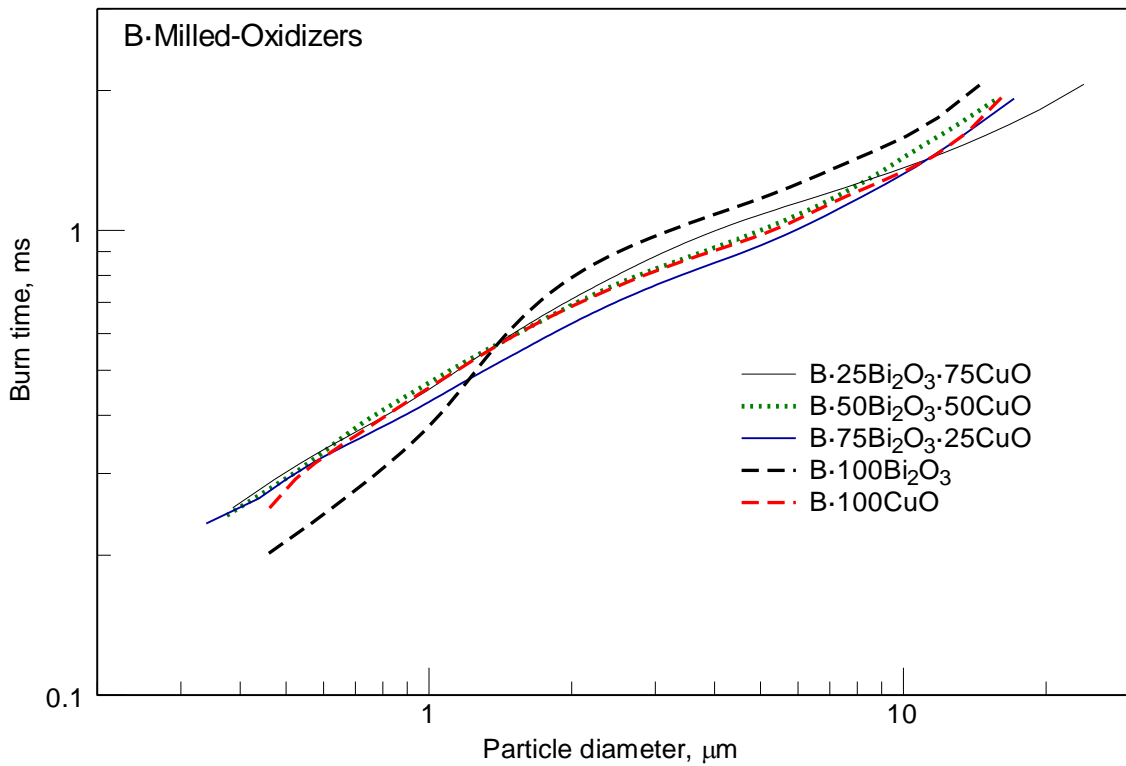


Figure 3.27 The burn time- particle size correlation for combustion in air of the prepared B-milled oxidizer samples.

CHAPTER 4

SUMMARY AND FUTURE WORK

This work was aimed to consider how milling conditions and compositions of the starting components affect characteristics of the inorganic materials processed by high-energy milling.

In the initial exploratory work, two powders, Bi_2O_3 and CuO were milled using 13 different fluids serving as PCAs. Crystallite size and particle size distributions of the milled powders were obtained using XRD and light diffraction, respectively. To streamline the analysis, the measurements were reduced to the surface moment mean diameter D_{50} and average crystallite size. These powder characteristics were correlated with multiple PCA properties using a linear model. Each powder characteristic was treated as a linear function of all PCA parameters; the correlation yielded coefficients for each parameter as well as respective intercept value. The models resulting in the lowest value of Akaike Information Criterion (AIC_c) function, $\delta\text{-AIC}_c$ and highest log likelihood (LogLik) value were considered as most suitable. These models were compared to one another considering which PCA characteristics they used and how well they predicted the experimental observations. No single PCA property has a determining effect on either of the powder characteristics. Such PCA properties as heat of vaporization, proton affinity, dipole moment, density and viscosity show some effect on both the sizes of powder particles and crystallites. Milling in acetonitrile and pyridine led to the smallest surface moment mean particle sizes for CuO and Bi_2O_3 respectively. On the other hand, the smallest crystallite sizes for both Bi_2O_3 and CuO were observed when the powders were milled in hexane.

For the future work, the experiments measuring zeta-potential and/or surface charge of a PCA-powder suspensions are of interest to analyze the PCA-powder physical

and chemical interactions. A high zeta-potential is expected to lead to a high suspension stability. The powder fluidization during milling would be substantially impacted by such the stability of the suspension, for example. Further surface modification due to PCA-powder interactions could lead to agglomeration or discretization of milling charge. Present work indicates that PCA properties are vital for understanding the milling process and obtaining targeted powder properties for future work. Thus, future efforts should be aimed at extending the present measurements, e.g., including experiments with different milling times for the same set of PCAs and adding zeta-potential measurements for the powder-PCA suspensions.

In the second part of this effort, an experimental study was conducted to pursue the effect of binary oxidizers ($\text{Bi}_2\text{O}_3 \cdot \text{CuO}$) on the ignition and combustion behavior of fuel-rich boron-binary oxidizer thermites ($\text{B} \cdot \text{Bi}_2\text{O}_3 \cdot \text{CuO}$) prepared by high-energy milling.

Two different methods were used to prepare the binary oxidizers. In the first method, commercially available metal oxides CuO and Bi_2O_3 were milled in hexane to produce ternary Bi-Cu-O compositions with different fractions of Bi and Cu. Micron-sized particles were obtained after milling. However, small amounts of unwanted phase in form of $(\text{BiO})_4\text{CO}_3(\text{OH})_2$ was observed in the obtained powders under XRD. In the second preparation method, commercially procured nitrates of Cu and Bi were mixed together and calcined. Coarse and agglomerated particles with target ternary compositions were synthesized as a result. Obtained powders were ball milled for size reduction. Highly homogeneous micron-sized composites were obtained when observed under SEM. Mixed oxide phase (Bi_2CuO_4) was observed in the compositions obtained from both preparatory

methods. Five different compositions with an increment of 25 wt. % Bi_2O_3 were prepared using both methods.

All obtained oxides were combined with boron by arrested reactive milling. During thermal analysis in an oxidizing environment, a mass gain and exothermic reaction were detected for all materials. The mass gain started at very low temperatures; the reaction later accelerated significantly. Composition B·25 Bi_2O_3 ·75CuO showed the maximum total measured mass gain amongst all the other compositions for both the composites milled and synthesized. The same composition also exhibited the highest rate of oxidation.

The ignition of the prepared compositions occurred in a narrow temperature range for all materials. Comparisons with thermo-analytical measurements show that the main oxidation step detected during low-heating rate experiments is irrelevant for ignition. Instead, ignition is apparently triggered by a weaker reaction detected at lower temperatures and resulting in a slow mass gain detected in TG traces. The composites containing higher fraction of Bi_2O_3 ignited at somewhat lower temperatures; the trend was especially clearly seen for powders with oxides synthesized by calcining mixed nitrates. It is likely that reduced Bi serves as shuttle catalyst more effectively than reduced Cu, leading to the respectively lower ignition temperatures. Apparently, presence of carbonates formed during milling made it more difficult to observe the effect of composition on the ignition temperature.

All prepared composite powders were fed into a focused CO_2 laser beam where they were ignited. The particles burned in air and their burn times were measured optically. For all materials, particle burn times were much shorter than for similarly sized particles

of elemental boron. However, no clear effect of the oxide composition on the burn time was detected.

The effect of the oxidizer composition could have been obscured for the prepared composite powders because of significant excess of boron fuel. Prepared reactive powders had an equivalence ratio of 21.6 for the boron-oxidizer redox reaction. At such a high equivalence ratio, the effect of oxidizer could have been critical for ignition. During combustion, this effect is expected due to the behavior of the reduced metal, Bi and/or Cu as shuttle catalyst, which oxidizes as a result of interaction with air and then instantly is reduced by boron. The difference in the reaction rates of Bi or Cu with surrounding oxygen at high temperatures may be difficult to detect in the present experiments. In future experiments, bulk energy release by the burning reactive powders with binary oxidizers should be assessed, e.g., using constant volume explosion experiments. Such measurements could be providing more insight into effectiveness of the binary oxidizers as improving characteristics of boron combustion.

CHAPTER 5

REFERENCES

1. Shang, X.; Wang, X.; Chen, S., Effects of Ball Milling Processing Conditions and Alloy Components on the Synthesis of Cu-Nb and Cu-Mo Alloys. *Materials (Basel)* 2019, *12* (8), 1224.
2. Zakeri, M.; Ramezani, M.; Nazari, A., Effect of ball to powder weight ratio on the mechanochemical synthesis of MoSi₂-TiC nanocomposite powder. *Materials Research* 2012, *15*, 891-897.
3. Kudaka, K.; Iizumi, K.; Sasaki, T.; Izumi, H., Effect of milling media on the reaction kinetics of the mechanochemical synthesis of pentatitanium trisilicide. *Journal of the American Ceramic Society* 2000, *83* (11), 2887-2889.
4. Cocco, G.; Delogu, F.; Schiffini, L., Toward a quantitative understanding of the mechanical alloying process. *Journal of Materials Synthesis and Processing* 2000, *8* (3-4), 167-180.
5. Delogu, F.; Mulas, G.; Schiffini, L.; Cocco, G., Mechanical work and conversion degree in mechanically induced processes. *Materials Science and Engineering A* 2004, *382* (1-2), 280-287.
6. Ward, T. S.; Chen, W.; Schoenitz, M.; Dreizin, E. L.; Dave, R. In *Nano-composite energetic powders prepared by arrested reactive milling*, Reno, NV, Reno, NV, 2005; pp 11049-11056.
7. Jiang, X.; Trunov, M. A.; Schoenitz, M.; Dave, R. N.; Dreizin, E. L., Mechanical alloying and reactive milling in a high energy planetary mill. *Journal of Alloys and Compounds* 2009, *478* (1-2), 246-251.

8. Santhanam, P. R.; Dreizin, E. L., Predicting conditions for scaled-up manufacturing of materials prepared by ball milling. *Powder Technology* 2012, *201*, 401-411.
9. Nouri, A.; Wen, C., Surfactants in mechanical alloying/milling: A catch-22 situation. *Critical Reviews in Solid State and Materials Sciences* 2014, *39* (2), 81-108.
10. Zolriasatein, A.; Yan, X.; Bauer, E.; Rogl, P.; Shokuhfar, A.; Paschen, S., Influence of PCA on thermoelectric properties and hardness of nanostructured Ba-Cu-Si clathrates. *Materials and Design* 2015, *87*, 883-890.
11. Machio, C.; Chikwanda, H.; Chikosha, S., Effect of process control agent (PCA) on the characteristics of mechanically alloyed Ti-Mg powders. *Journal of the Southern African Institute of Mining and Metallurgy* 2011, *111* (3), 149-153.
12. Pans, M. A.; Gayán, P.; Abad, A.; García-Labiano, F.; de Diego, L. F.; Adánez, J., Use of chemically and physically mixed iron and nickel oxides as oxygen carriers for gas combustion in a CLC process. *Fuel Processing Technology* 2013, *115*, 152-163.
13. Lee, H. J.; Back, S.; Lee, J. H.; Choi, S. H.; Jung, Y.; Choi, J. W., Mixed Transition Metal Oxide with Vacancy-Induced Lattice Distortion for Enhanced Catalytic Activity of Oxygen Evolution Reaction. *ACS Catalysis* 2019, *9* (8), 7099-7108.
14. Petrantoni, M.; Rossi, C.; Salvagnac, L.; Conédéra, V.; Estève, A.; Tenailleau, C.; Alphonse, P.; Chabal, Y. J., Multilayered Al/CuO thermite formation by reactive magnetron sputtering: Nano versus micro. *Journal of Applied Physics* 2010, *108* (8).
15. Reese, D. A.; Wright, D. M.; Son, S. F., CuO/Al thermites for solid rocket motor ignition. *Journal of Propulsion and Power* 2013, *29* (5), 1194-1199.

16. Sanders, V. E.; Asay, B. W.; Foley, T. J.; Tappan, B. C.; Pacheco, A. N.; Son, S. F., Reaction propagation of four nanoscale energetic composites (Al/MO₃, Al/WO₃, Al/CuO, and Bi₂O₃). *Journal of Propulsion and Power* 2007, 23 (4), 707-714.
17. Huang, S.; Deng, S.; Jiang, Y.; Zheng, X., Experimental effective metal oxides to enhance boron combustion. *Combustion and Flame* 2019, 205, 278-285.
18. Dutro, G. M.; Yetter, R. A.; Risha, G. A.; Son, S. F., The effect of stoichiometry on the combustion behavior of a nanoscale Al/MO₃ thermite. *Proceedings of the Combustion Institute* 2009, 32 II, 1921-1928.
19. Valluri, S. K.; Monk, I.; Schoenitz, M.; Dreizin, E., Fuel-rich aluminum–metal fluoride thermites. *International Journal of Energetic Materials and Chemical Propulsion* 2017, 16 (1), 81-101.
20. Ward, T. S.; Trunov, M. A.; Schoenitz, M.; Dreizin, E. L., Experimental methodology and heat transfer model for identification of ignition kinetics of powdered fuels. *International Journal of Heat and Mass Transfer* 2006, 49 (25-26), 4943-4954.
21. Valluri, S. K.; Schoenitz, M.; Dreizin, E., Boron-metal fluoride reactive composites: Preparation and reactions leading to their ignition. *Journal of Propulsion and Power* 2019, 35 (4), 802-810.
22. Corcoran, A.; Mercati, S.; Nie, H.; Milani, M.; Montorsi, L.; Dreizin, E. L., *Combustion of Fine Aluminum and Magnesium Powders in Water* 2013, 160, 155-160.
23. Mohan, S.; Trunov, M. A.; Dreizin, E. L., Heating and ignition of metallic particles by a CO₂ laser. *Journal of Propulsion and Power* 2008, 24 (2), 199-205.

24. Chintersingh, K. L.; Schoenitz, M.; Dreizin, E. L., Combustion of boron and boron–iron composite particles in different oxidizers. *Combustion and Flame* 2018, *192*, 44-58.
25. Tsang, C.-F.; Meen, J. K.; Elthon, D., Phase Equilibria of the Bismuth Oxide-Copper Oxide System in Oxygen at 1 atm. *Journal of the American Ceramic Society* 1994, *77* (12), 3119-3124.